Two forms of autosomal dominant primary retinitis pigmentosa

R.W. MASSOF and D. FINKELSTEIN

Wilmer Ophthalmological Institute, The Johns Hopkins University School of Medicine, Baltimore, MD 21205, USA

Keywords: retinitis pigmentosa, inherited retinal degenerations, absolute thresholds, spectral sensitivity, static perimetry, electroretinogram

Abstract. Two types of autosomal dominant retinitis pigmentosa (RP) are identified on the basis of perimetric measures of rod sensitivity relative to cone sensitivity. Type 1 dominant RP patients are characterized by an early diffuse loss of rod sensitivity with a later loss of cone sensitivity and by childhood onset of nightblindness. Type 2 dominant RP patients are characterized by a regionalized and combined loss of rod and cone sensitivity with adulthood onset of nightblindness. Comparisons of losses in the photopic and scotopic electroretinogram amplitudes corroborate the psychophysical results. Clinical findings are similar for the two dominant RP subtypes, however, there are differences in natural history.

Introduction

Primary retinitis pigmentosa (RP) is a clinically defined syndrome. The most consistent signs and symptoms are: (1) nightblindness, (2) ring-like scotoma or visual field contractions, (3) midperipheral intraretinal bone-spicule-like pigmentation, (4) narrowed retinal arterioles, (5) preservation of good visual acuity until late in the course of the disease, and (6) degeneration of the vitreous. Although many retinal degenerations meet several, or all of these clinical criteria, the diagnosis of primary RP is reserved for those retinal degenerations that cannot be attributed to inflammatory, toxic, traumatic, or systemic metabolic causes. Thus, primary RP is defined by a process of exclusion, and all cases are idiopathic, although 50% to 60% of cases are familial (e.g., Jay, 1972).

It is assumed that all cases of primary RP are inherited in one of three ways: autosomal dominant, autosomal recessive, or X-linked recessive. The plurality of RP cases have no family history of RP, but, they are presumed to be hereditary.

Although it is widely assumed that RP can be classified into homogeneous groups according to the mode of inheritance, homogeneity of the genetic

Supported by research grants from the U.S. Public Health Service, National Institutes of Health (EY-01791) and the National Retinitis Pigmentosa Foundation.
Reprint requests: Robert W. Massof, Ph.D., Wilmer Institute, B-34, The Johns Hopkins Medical Institutions, 600 N. Wolfe Street, Baltimore, Maryland 21205, USA

Documenta Ophthalmologica 51, 289–346 (1981) 0012–4486/81/0514–0289 $8.70

groups has never been demonstrated. Indeed, within the genetic categories, the high degree of RP variability as regards onset age and natural history (Hussels-Maumenee et al., 1975; Palmer, Massof & Finkelstein, 1980) may reflect heterogeneity of disease mechanisms. Recognizing this possibility, Krill (1972) recommended that recessive RP be divided into early and late onset groups. Massof & Finkelstein (1979a) argued that both dominant and recessive RP may encompass several different disease forms, primarily differing in the relation of rod sensitivity to cone sensitivity. On the basis of electroretinography (ERG) data, Marmor (1979) also suggested that subgroups of both dominant and recessive RP may exist. Berson and colleagues (1968, 1969) suggested that dominant RP may be divided into two groups on the basis of gene penetrance (viz. full and reduced) and stated that the temporal characteristics of the ERG differ for the two subtypes.

The present paper is an extension of our earlier work which illustrates that RP patients can be classified on the basis of rod sensitivity loss relative to cone sensitivity loss throughout the visual field (Massof & Finkelstein, 1979a). In the present study, we further examine rod and cone function in 25 RP patients, representing 13 autosomal dominant pedigrees, and demonstrate that there are at least two forms of autosomal dominant RP, with different natural histories and apparently different disease mechanisms.

Two-color dark-adapted sensitivity profiles

The identification of dominant RP subtypes is based on static perimetric measures that reflect dark-adapted spectral sensitivity. This method of evaluating rod and cone function in RP was first employed by Zeavin & Wald (1956) and was later extended by Massof & Finkelstein (1979a). In brief, to evaluate rod sensitivity relative to cone sensitivity, we have taken advantage of the difference between rod and cone spectral sensitivities.

It is not practical to measure the complete spectral sensitivity function at every retinal position in order to identify rod and cone contributions to stimulus detection. However, the ratios of sensitivities to a short-wavelength stimulus (500 nm) and a long-wavelength stimulus (650 nm) will serve to identify the absolute threshold spectral sensitivity if the shapes of the underlying rod and cone functions are known.

For most retinal positions in normal subjects, absolute thresholds for stimuli of different spectral composition will be determined by scotopic spectral sensitivity, i.e., the rod system (Johnson & Massof, 1980; Stabell & Stabell, 1981). Figure 1a illustrates the scotopic spectral sensitivity curve. When thresholds are determined by the scotopic system, about 3 log units more energy is required to detect a 650 nm stimulus than is required to detect a 500 nm stimulus.

If the scotopic system could be eliminated (e.g., by rod degeneration) the absolute thresholds for stimuli of different spectral composition would be determined by photopic spectral sensitivity, i.e., the cone system. Figure 1b

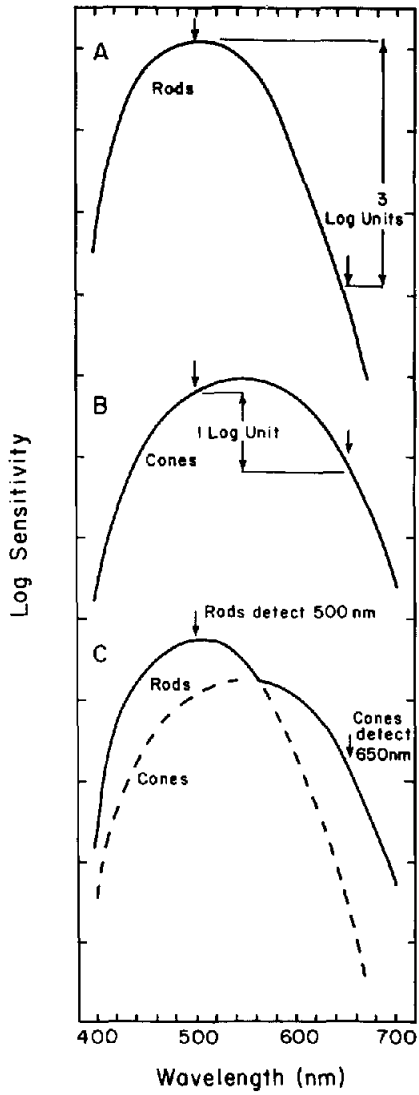

Figure 1. (a) Spectral sensitivity of the rods (C.I.E. scotopic luminosity function). As indicated by the arrows, the rod system is 3 log units more sensitive to a 500 nm stimulus than to a 650 nm stimulus. (b) Spectral sensitivity of the cone system (C.I.E. photopic luminosity function corrected for the lack of macular pigment). As indicated by the arrows, the cones are 1 log unit more sensitive to a 500 nm stimulus than to a 650 nm stimulus. (c) If the rod and cone spectral sensitivity functions overlap, the rods will detect the 500 nm stimulus and the cones will detect the 650 nm stimulus. In this case, the difference between log sensitivities will fall between 1 and 3 log units.

illustrates the photopic spectral sensitivity curve. When thresholds are determined by the photopic system, about 1 log unit more energy is required to detect a 650 nm stimulus than is required to detect a 500 nm stimulus.

Luminance is simply a correction of radiance for photopic spectral sensitivity. Therefore, by definition, if the photopic system is responsible for stimulus detection at absolute threshold, the threshold luminances for 500 nm and 650 nm would be the same; if the scotopic system is responsible for detection at absolute threshold, the threshold luminance for 650 nm would be 2 log units greater than the threshold luminance for 500 nm.

Working in luminance units, a measured threshold difference of 2 log units between stimuli of 650 nm and 500 nm shows that the scotopic system mediated the detection, a measurement of no difference between the threshold luminances for the same two stimuli shows that the photopic system mediated detection. If a difference value between 0 and 2 log units was obtained, we would conclude that the scotopic system was responsible for detecting the 500 nm stimulus and the photopic system was responsible for detecting the 650 nm stimulus. This latter conclusion assumes a threshold spectral sensitivity curve similar to the example in Figure 1c.

The above arguments are supported by dark-adaptation measures in the peripheral retina (20° nasal field) for long and short wavelength stimuli (λ_{max} = 650 nm and 500 nm, respectively). These data, reported previously (Massof & Finkelstein, 1979a) and reproduced in Figures 2a and 2b, indicate a threshold luminance difference of 3 log units between the rod and cone plateaus for the short-wavelength stimulus (Fig. 2, top) and a threshold luminance difference of 0.5 log unit between the rod and cone plateaus for the long-wavelength stimulus (Fig. 2, bottom). Thus, after full dark adaptation, for this retinal position, the rod system detected both stimuli. Subtracting the short-wavelength log threshold luminance from the long-wavelength log threshold luminance, the final dark-adapted log threshold luminance difference is at the expected rod level of 2 log units. At the cone threshold plateau (e.g., 8 min) the log threshold luminance difference is −0.3 (long-wavelength stimulus has lower threshold luminance than the short-wavelength stimulus). This disagreement with the expectation of zero threshold luminance difference for cones is consistent with previously measured departures of foveal absolute-threshold spectral sensitivity from photopic spectral luminosity (Guth & Lodge, 1973).

Our experimental technique for studying RP patients consisted of measuring absolute thresholds for the short and long-wavelength stimuli at various positions throughout the visual field. In order to interpret these threshold measures in terms of rod and cone sensitivities, we have developed a simulation model. The model generates predictions of the differences between log threshold luminances for the two different color stimuli as a function of the relation of rod sensitivity to cone sensitivity.

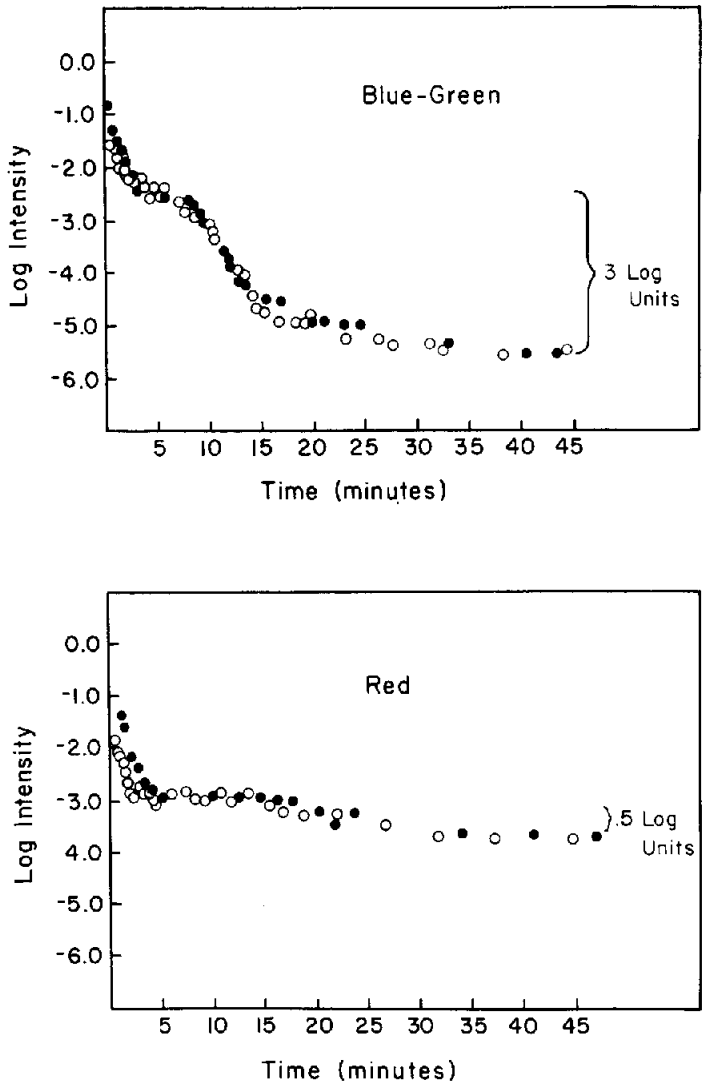

Figure 2. (Top) Dark adaptation curve measured at 20° nasal for two observers (open and closed symbols) using a short-wavelength target. The difference between the rod and cone plateaus is 3 log units. (Bottom) Dark adaptation curves measured at the same retinal position, for the same two observers, employing a long-wavelength stimulus. The rod and cone break occurs at 15 minutes, and the difference between the rod and cone plateaus is 0.5 log units.

Simulation model

The two-color threshold simulation model is based on two empirical parameters: (1) the measured difference between the log threshold luminances

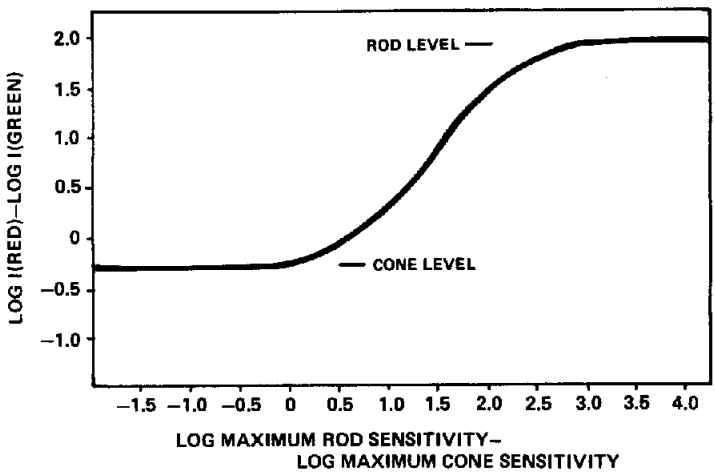

Figure 3. Difference between log threshold luminance for the long-wavelength stimulus and log threshold luminance for the short-wavelength stimulus plotted as a function of the difference between the log maximum rod sensitivity and log maximum cone sensitivity. These data were computed from dark adaptation curves, such as those in Figure 2 and from rod and cone spectral sensitivity curves (cf. Fig. 1).

for the two stimuli for rods and for cones and (2) the measured difference between maximum rod sensitivity and maximum cone sensitivity as a function of retinal position. The assumptions of the models are: (1) the most sensitive receptor system will mediate detection and (2) rod and cone spectral sensitivities do not appreciably change with retinal position. The first assumption ignores putative rod-cone interactions and probability summation. The second assumption is well supported by the work of Wooten et al. (1975) and our earlier measures of peripheral absolute threshold spectral sensitivity in normal subjects and RP patients (Massof, Johnson & Finkelstein, 1981).

From data such as those in Figure 2, we can compute the expected difference between the dark-adapted threshold luminances for the long and short-wavelength stimuli as a function of the difference between the maximum sensitivities of the rod and cone systems. This function is illustrated in Figure 3. As indicated by the lower bar, the expected difference between the log threshold luminances will have the cone spectral sensitivity determined value of -0.3 if the rod and cone systems have the same maximum sensitivities (0 log unit difference) or if the maximum rod sensitivity is less than the maximum cone sensitivity. On the other hand, as indicated by the upper bar, a rod spectral-sensitivity-determined log threshold luminance difference of 2 is expected if the maximum rod-system sensitivity exceeds the maximum cone-system sensitivity by 3 log units, or more.

To simulate perimetric measures of the difference between dark-adapted log threshold luminances for the long and short-wavelength stimuli, it is necessary to have an estimate of the normal perimetric differences between

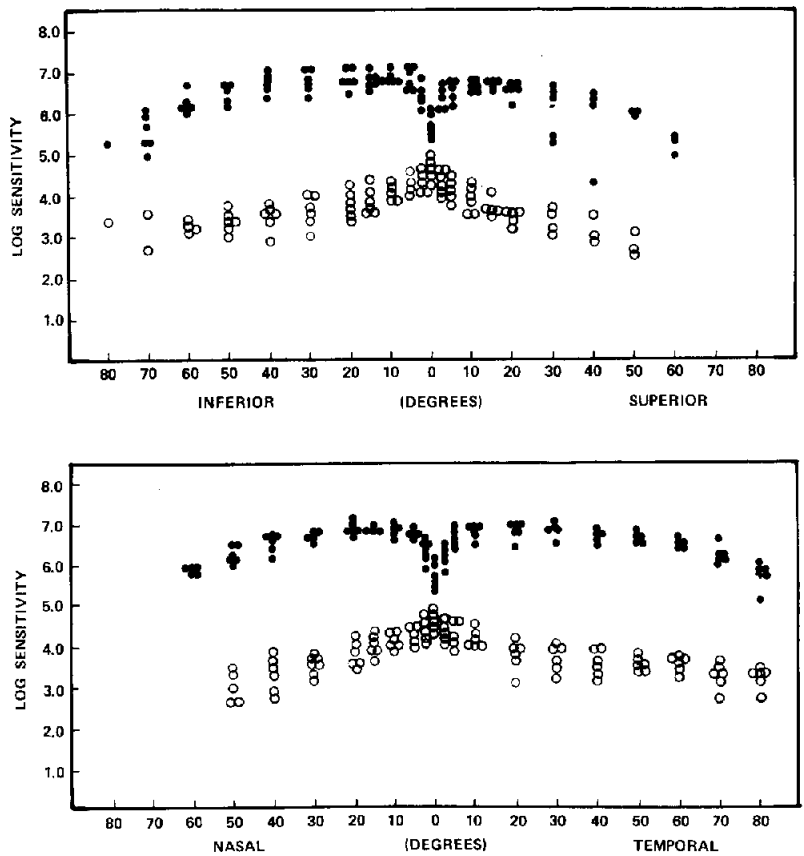

Figure 4. Log sensitivities at absolute threshold for rods (filled circles) and cones (open circles) are plotted as a function of retinal eccentricity for the vertical meridian (top panel) and horizontal meridian (bottom panel) for six normal observers. These data, taken from Fitzke & Massof (1980), provide the estimates for the difference between maximum rod sensitivity and maximum cone sensitivity (listed in Table 1).

maximum rod and cone sensitivities. Such an estimate is available from an earlier study (Fitzke & Massof, 1980); the data for the horizontal and vertical meridians are reproduced in Figure 4. The filled circles may be regarded as log rod-system sensitivities, and the open circles as log cone-system sensitivities at the same retinal positions. By averaging the rod system data at each retinal position and subtracting the average of the corresponding cone system data, the differences between rod and cone system log sensitivities are obtained. Because the data in Figure 4 were obtained with a 2° white stimulus, a correction constant was added for spectral sensitivity. The resulting values, which now represent estimates of the difference between maximum rod and cone sensitivities, as a function of retinal position, are listed in Table 1. The corresponding expected values for the difference between dark-adapted log

Table 1.

Eccentricity	Log maximum rod sensitivity– Log maximum cone sensitivity	Log I (red)– Log I (blue-green)
80° temporal	2.65	1.9
70° temporal	3.05	1.9
60° temporal	3.15	1.9
50° temporal	3.25	1.9
40° temporal	3.35	1.9
30° temporal	3.15	1.9
20° temporal	3.15	1.9
10° temporal	2.85	1.9
5° temporal	2.55	1.85
2.5° temporal	2.25	1.6
0°	1.35	0.6
2.5° nasal	2.15	1.5
5° nasal	2.45	1.8
10° nasal	2.95	1.9
15° nasal	3.15	1.9
20° nasal	3.25	1.9
30° nasal	3.45	1.9
40° nasal	3.55	1.9
50° nasal	3.55	1.9

threshold luminances for the long and short-wavelength stimuli, from the function in Figure 3, also are listed in Table 1.

The maximum rod-cone sensitivity difference values as a function of field position that are listed in Table 1, and the function in Figure 3, constitute the simulation model for evaluating data obtained on RP patients. To test the model, three experiments were performed on normal observers.

Methods

For the first experiment, following 45 minutes of dark adaption, absolute thresholds were measured at the fovea and at 2.5°, 5°, 10°, 15° and from 20° through 80° in 10° steps along the nasal and temporal meridians, employing the Tubinger perimeter. Thresholds were measured for both a short-wavelength (λ_{max} = 500 nm; maximum luminance = 72 cd/m^2) and a long-wavelength (λ_{max} = 650 nm; maximum luminance = 91 cd/m^2) stimulus, subtending a visual angle of 2°, and flashed for a duration of 500 msec. Threshold was defined as the mean of 3 to 5 repetitions of an ascending method of limits.

For the second and third experiments, measures were taken similarly at the same field positions on a 3.2 cd/m^2 green (λ_{max} = 530 nm) ganzfeld background and a 34 cd/m^2 white ganzfeld background, respectively. These latter measures were increment thresholds because the test stimuli were superimposed on the background.

Results

Log sensitivities at absolute threshold (relative to maximum luminance) for

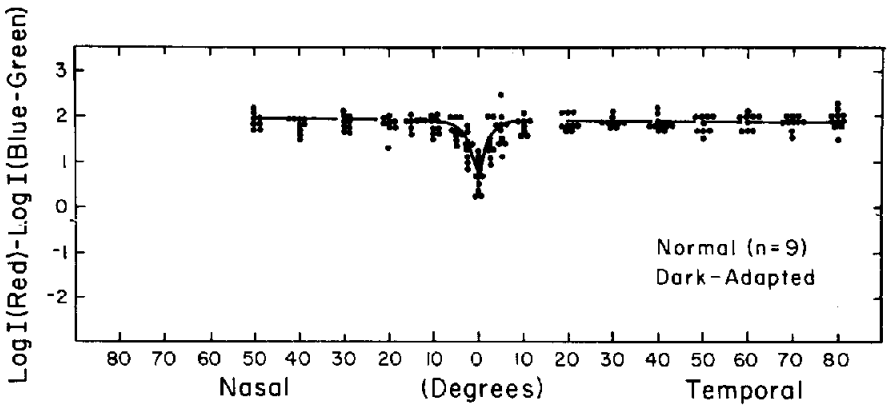

Figure 5. Values for difference between log absolute threshold luminance for the red light and log absolute threshold luminance for the blue-green light are plotted as a function of retinal eccentricity along the horizontal meridian for 9 normal observers (filled circles). The solid line plotted along with the data is the prediction from the simulation model (cf. Table 1).

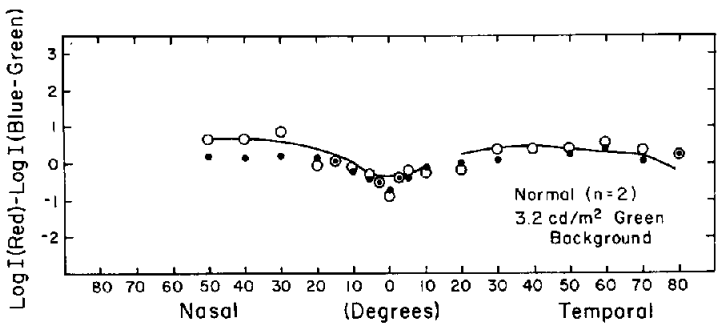

Figure 6. Differences between log increment threshold luminances for the long-wavelength and short-wavelength stimuli on the 3.2 cd/m^2 green background are plotted for 2 normal observers (filled and open circles), as a function of retinal eccentricity along the horizontal meridian. The solid line fit to the data is the prediction of the simulation model assuming a 2.2 log unit reduction in rod sensitivity relative to cone sensitivity. That is, 2.2 was subtracted from every value in the second column of Table 1, and new log threshold luminance difference values were computed from the function in Figure 3.

9 normal subjects, ranging in age from 25 to 62 years, were obtained as a function of visual field position for the short and long-wavelength stimuli. For each field position, the log threshold luminance for the short-wavelength stimulus was subtracted from the log threshold luminance for the long-wavelength stimulus. These log threshold luminance differences, which reflect threshold spectral sensitivity, are plotted as a function of field eccentricity in Figure 5. The solid line along with the difference values in Figure 5 is the prediction from the simulation model (see Table 1).

Differences between log sensitivities for the short and long-wavelength

increment thresholds on the 3.2 cd/m^2 green background, for 2 normal observers, are plotted as a function of eccentricity in Figure 6. The solid line fit to the difference values in Figure 6 is the prediction of the simulation model. assuming the green background suppressed the rod-system sensitivity 2.2 log units more than it suppressed the cone-system sensitivity; that is, 2.2 was subtracted from every value in the second column of Table 1 (difference between maximum rod and cone log sensitivities), and the expected values for the differences between the log threshold luminances of the short and long-wavelength stimuli were recomputed from the function in Figure 6.

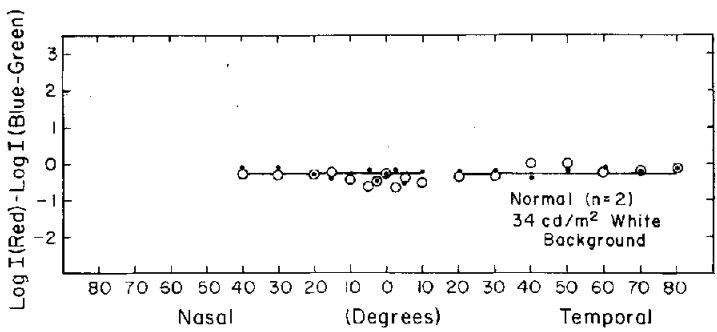

Figure 7. Same as Figure 6, but plotted for increment thresholds on a 34 cd/m^2 white background. The solid line fit to the data points is the prediction of the simulation model assuming there were no rod contributions to the increment thresholds (i.e., at least 3.2 log unit reduction in rod sensitivity relative to cone sensitivity).

Differences between log sensitivities for the short and long wavelength increment thresholds on the 34 cd/m^2 white background, for 2 normal observers, are plotted as a function of eccentricity in Figure 7. The solid line fit to the data is the prediction from the simulation model, assuming the white background suppressed the rod-system sensitivity at least 3.2 log units more than it suppressed the cone-system sensitivity; i.e., cone-system difference values are predicted for each retinal position.

Comments

In this section we have developed and tested the analytic tools needed to evaluate perimetric threshold measures for the short and long-wavelength stimuli in RP patients. The simulation model permits determination of relative involvements of the rod and cone systems in retinal disease.

Subtypes of autosomal dominant RP

Two-color dark-adapted sensitivity profiles* were obtained from 25 RP patients. For all patients, with the exceptions of patients F1 and F2, an

*Profile refers to static measures of visual function along a single meridian.

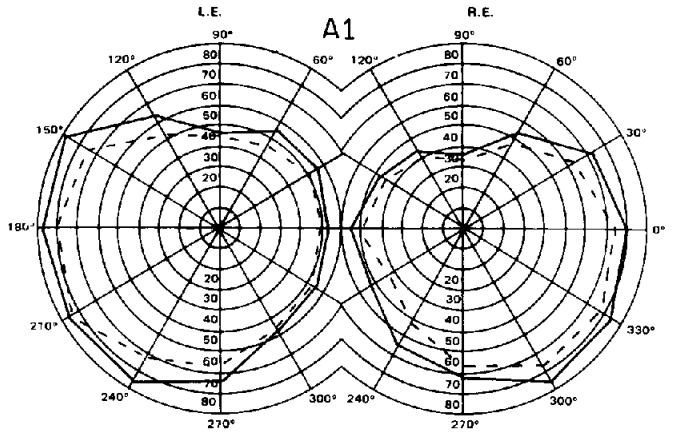
L.E.
R.E.
A1
90°
120°
60°
150°
30°
180°
0°
210°
330°
240°
300°
270°
80
70
60
50
40
30
20

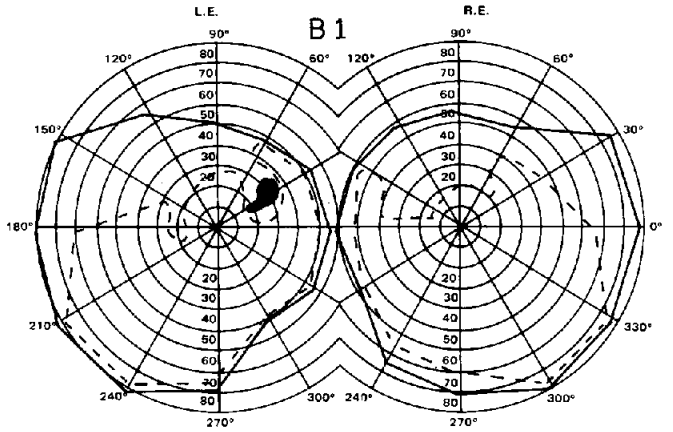
L.E.
R.E.
B 1
90°
120°
60°
150°
30°
180°
0°
210°
330°
240°
300°
270°
80
70
60
50
40
30
20

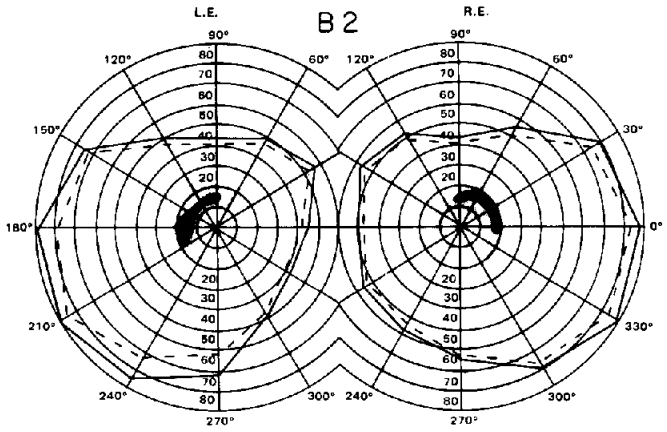
L.E.
R.E.
B 2
90°
120°
60°
150°
30°
180°
0°
210°
330°
240°
300°
270°
80
70
60
50
40
30
20

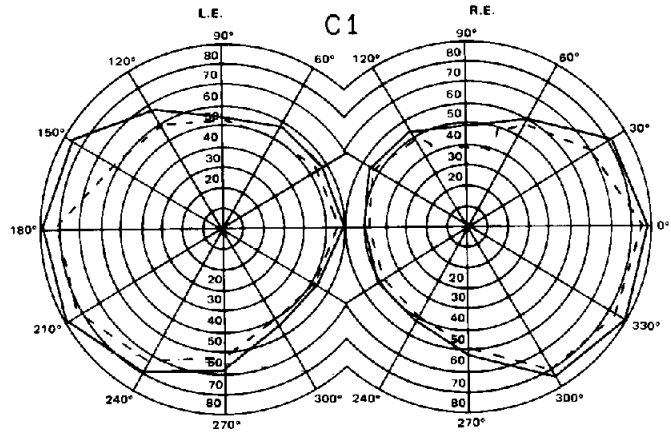
C1
L.E.
R.E.
90°
60°
120°
30°
150°
180°
0°
210°
330°
240°
300°
270°
80
70
60
50
40
30
20

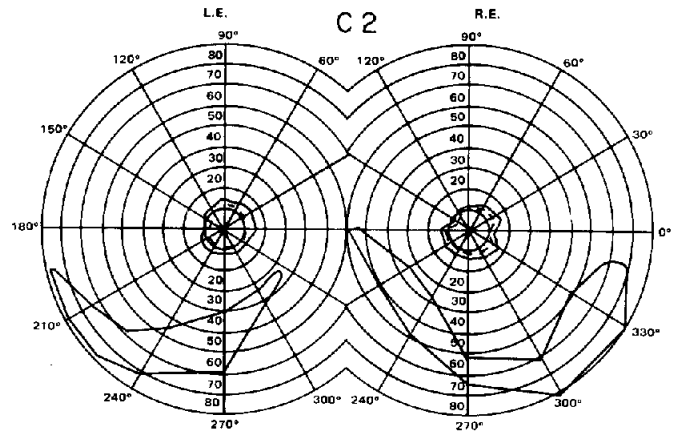
C2
L.E.
R.E.
90°
60°
120°
30°
150°
180°
0°
210°
330°
240°
300°
270°
80
70
60
50
40
30
20

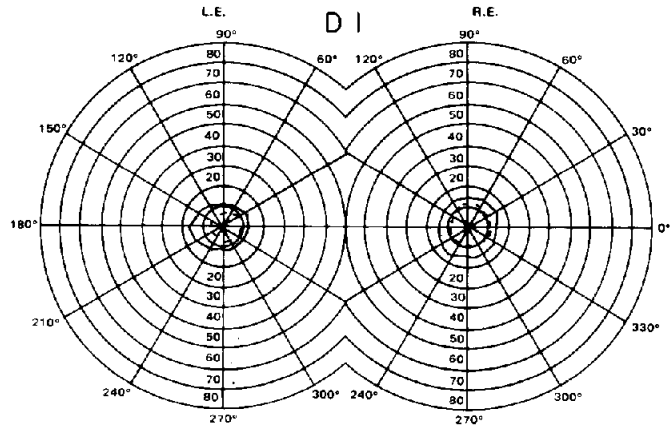
D I
L.E.
R.E.
90°
60°
120°
30°
150°
180°
0°
210°
330°
240°
300°
270°
80
70
60
50
40
30
20

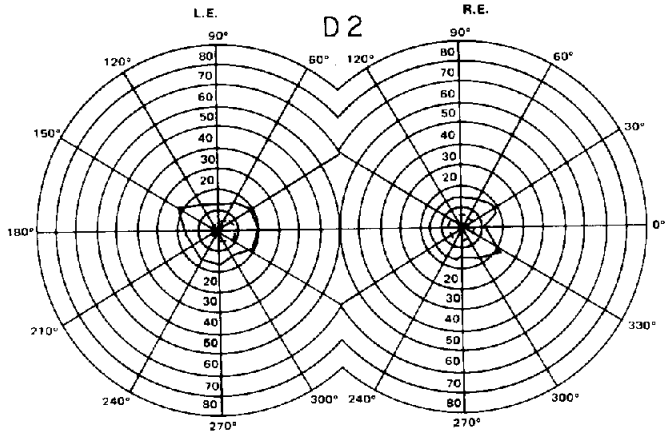
L.E.
D2
R.E.
90°
120°
60°
150°
30°
180°
0°
210°
330°
240°
300°
270°
80
70
60
50
40
30
20

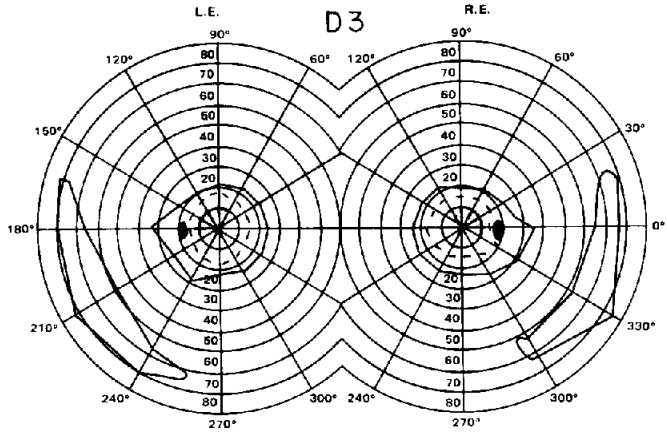
L.E.
D3
R.E.
90°
120°
60°
150°
30°
180°
0°
210°
330°
240°
300°
270°
80
70
60
50
40
30
20

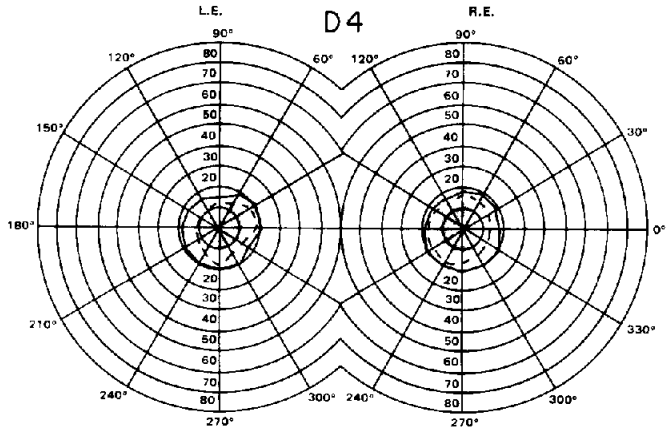
L.E.
D4
R.E.
90°
120°
60°
150°
30°
180°
0°
210°
330°
240°
300°
270°
80
70
60
50
40
30
20

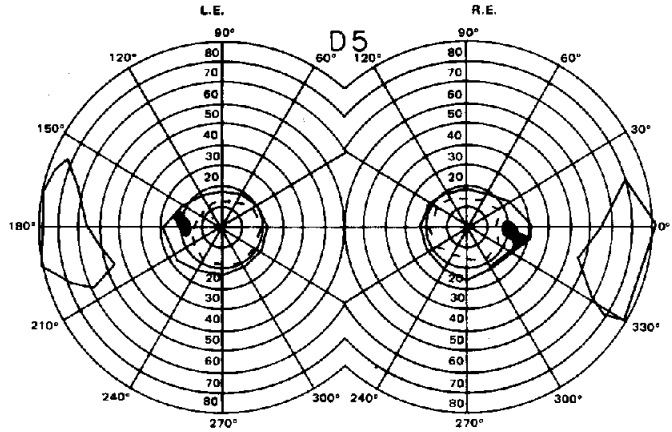
L.E.
R.E.
D5
90°
120°
60°
150°
30°
180°
0°
210°
330°
240°
300°
270°
20
30
40
50
60
70
80

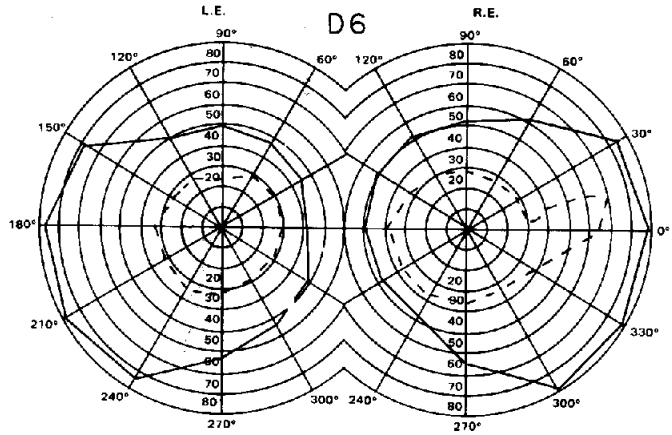
L.E.
R.E.
D6
90°
120°
60°
150°
30°
180°
0°
210°
330°
240°
300°
270°
20
30
40
50
60
70
80
90

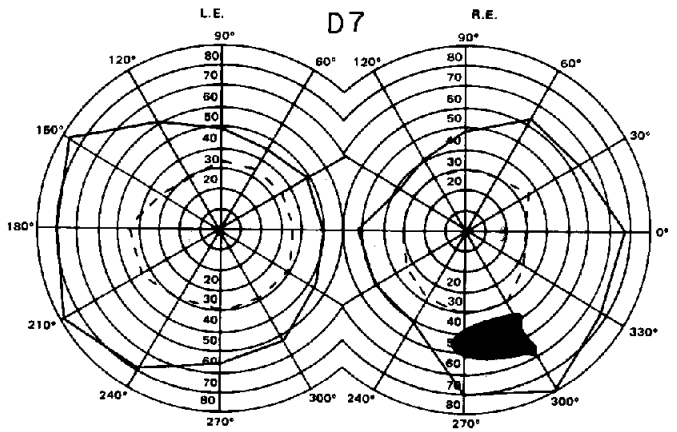
L.E.
R.E.
D7
90°
120°
60°
150°
30°
180°
0°
210°
330°
240°
300°
270°
20
30
40
50
60
70
80

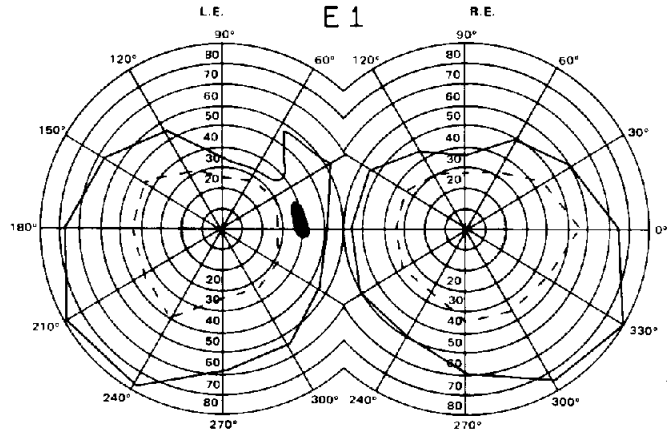
E 1
L.E.
R.E.
90°
60°
120°
30°
150°
180°
0°
210°
330°
240°
300°
270°
20
30
40
50
60
70
80

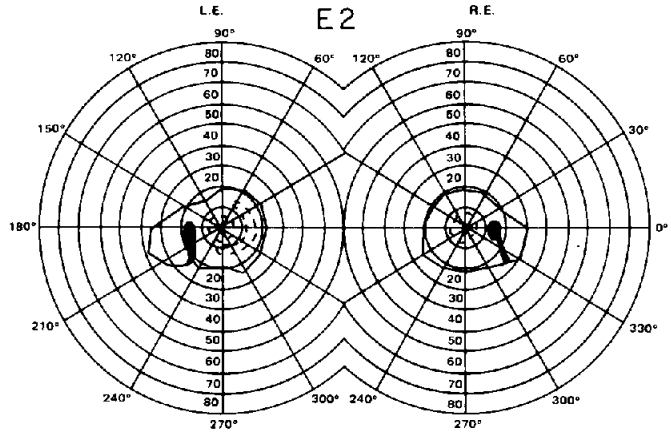
E 2
L.E.
R.E.
90°
60°
120°
30°
150°
180°
0°
210°
330°
240°
300°
270°
20
30
40
50
60
70
80

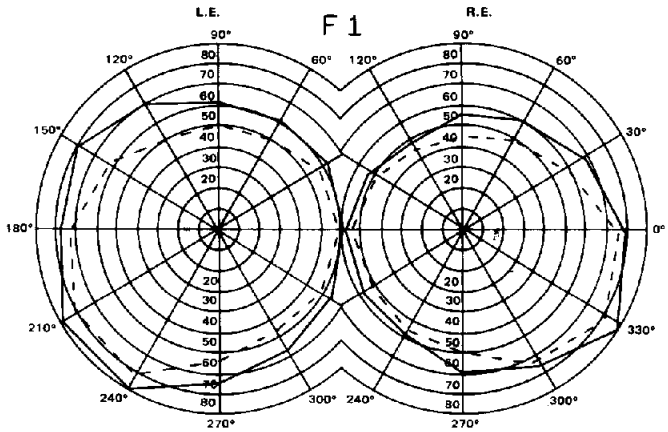
F 1
L.E.
R.E.
90°
60°
120°
30°
150°
180°
0°
210°
330°
240°
300°
270°
20
30
40
50
60
70
80

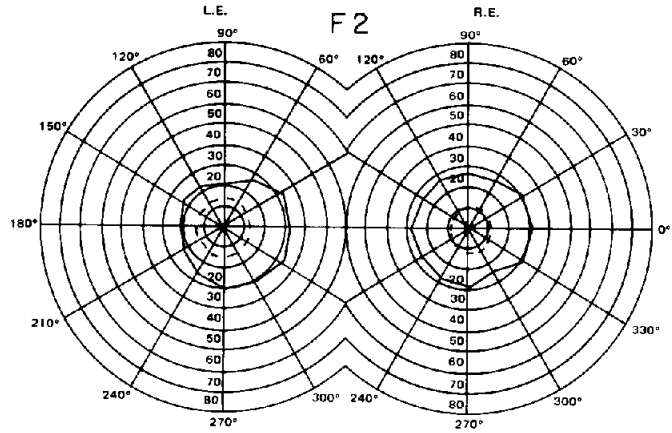
L.E.
F 2
R.E.
90°
120°
60°
150°
30°
180°
0°
210°
330°
240°
300°
270°
10
20
30
40
50
60
70
80

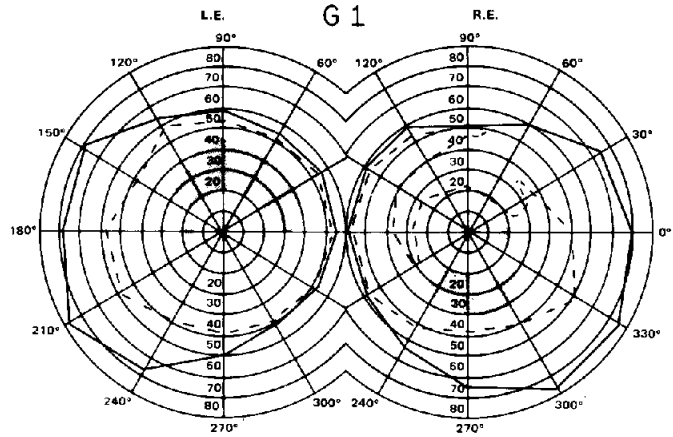
L.E.
G 1
R.E.
90°
120°
60°
150°
30°
180°
0°
210°
330°
240°
300°
270°
10
20
30
40
50
60
70
80

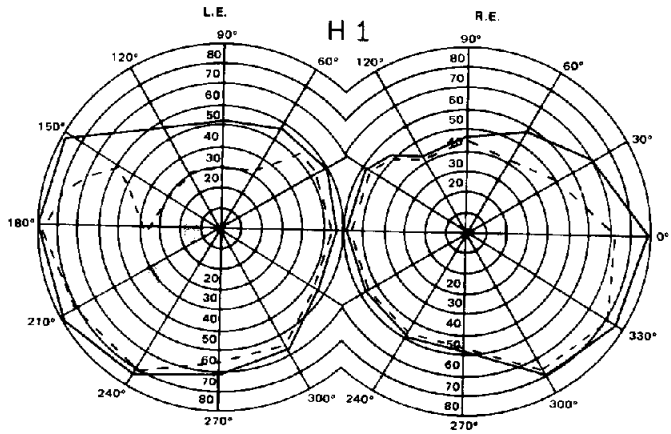
L.E.
H 1
R.E.
90°
120°
60°
150°
30°
180°
0°
210°
330°
240°
300°
270°
10
20
30
40
50
60
70
80

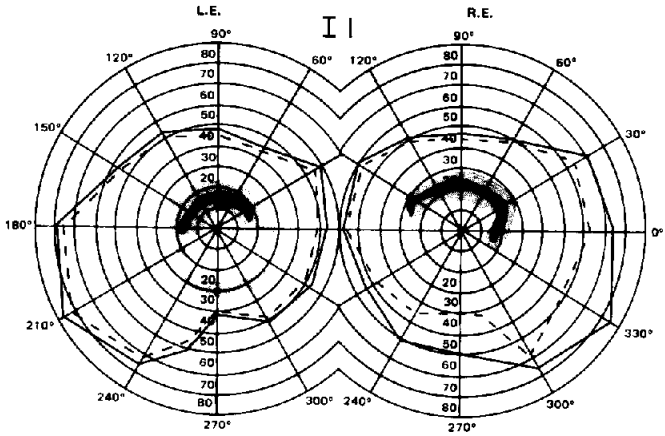
I 1
L.E.
R.E.
90°
120°
60°
150°
30°
180°
0°
210°
330°
240°
300°
270°
80
70
60
50
40
30
20

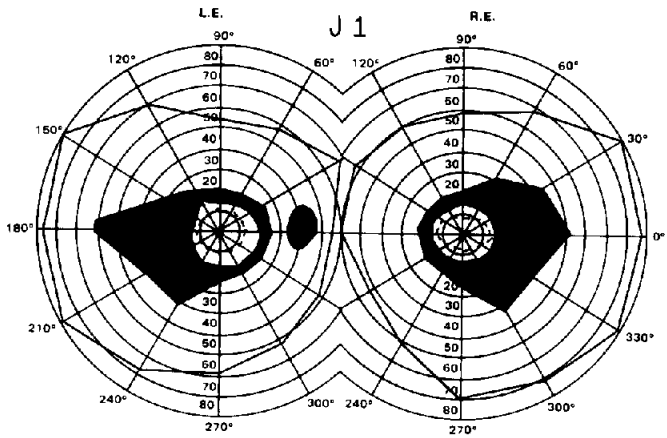
J 1
L.E.
R.E.
90°
120°
60°
150°
30°
180°
0°
210°
330°
240°
300°
270°
80
70
60
50
40
30
20

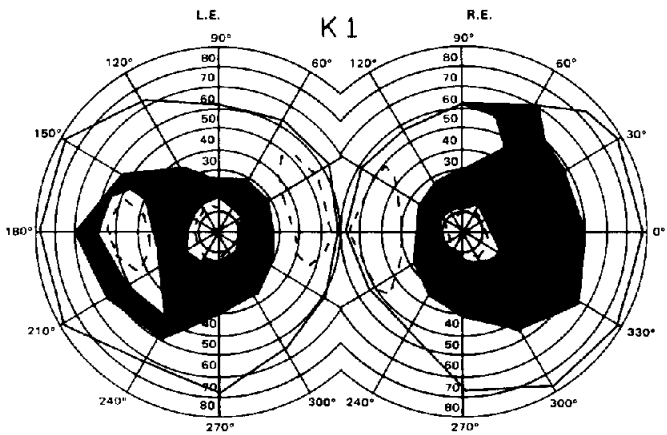
K 1
L.E.
R.E.
90°
120°
60°
150°
30°
180°
0°
210°
330°
240°
300°
270°
80
70
60
50
40
30

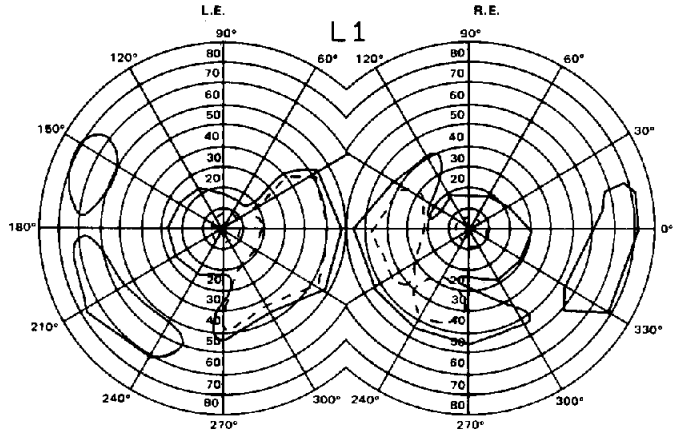
L.E.
R.E.
L1
90°
120°
60°
150°
30°
180°
0°
210°
330°
240°
300°
270°
10
20
30
40
50
60
70
80

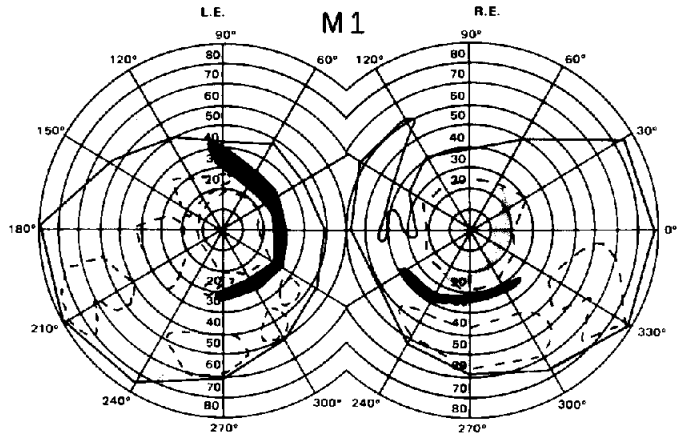
L.E.
R.E.
M1
90°
120°
60°
150°
30°
180°
0°
210°
330°
240°
300°
270°
10
20
30
40
50
60
70
80

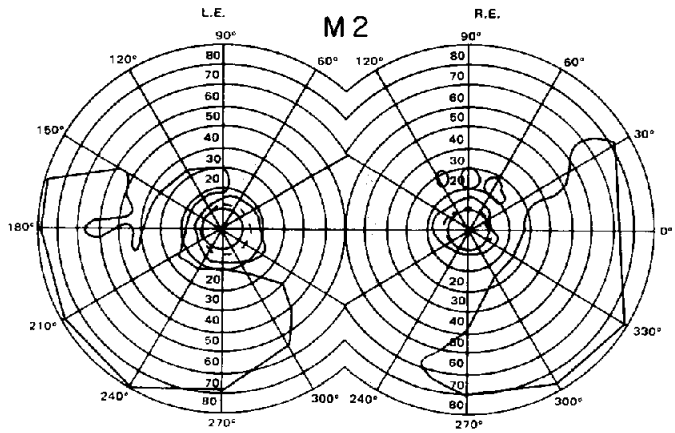
L.E.
R.E.
M2
90°
120°
60°
150°
30°
180°
0°
210°
330°
240°
300°
270°
10
20
30
40
50
60
70
80

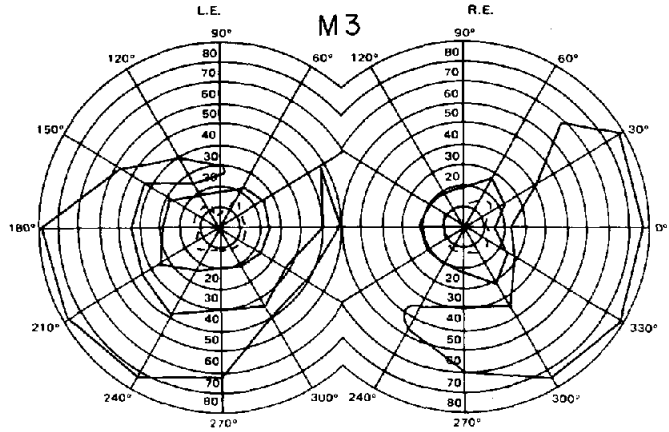

Figure 8. Visual fields measured on the Goldmann perimeter with the V/4 (solid line) and II/4 (dashed line) targets. Black areas denote scotomas to the V/4 target, and shaded areas denote scotomas to the II/4 target.

autosomal dominant pattern of inheritance extended over three generations, or more. Patient F1 is the son of patient F2; and although the mode of inheritance in their cases is indeterminate, they are included as a possible autosomal dominant pedigree. Patients B1 and B2 are brothers, patient C1 is the daughter of patient C2, patients D1 through D5 are siblings, patient D6 is the son of patient D3 and patient D7 is the daughter of patient D4, patient E1 is the daughter of patient E2, and patient M2 is the father of patient M1 and the brother of patient M3.

Clinical examinations were performed on all patients. Procedures included: (1) measures of visual acuity, (2) measures of color discrimination with the Farnsworth-Munsell 100 hue test using a MacBeth illuminant, (3) measures of visual fields for the V/4 and II/4 targets employing a Goldmann perimeter, (4) fundus examination, (5) slit lamp examination, (6) measures of the electroretinogram in response to ganzfeld stimulation, (7) measures of the electrooculogram (EOG) light-dark (Arden) ratio, and (8) determination of auditory function by measures of pure tone thresholds from 250 Hz to 8,000 Hz.

The clinical characteristics of the patients are listed in Table 2; their visual fields are illustrated in Figure 8. All patients had the typical RP signs and symptoms except patients C1 and F1. Patient C1 had no intraretinal bone-spicule pigmentation, however, she had narrowed arterioles, vitreous degeneration and other typical RP features. Patient F1 also had vitreous degeneration but no pigment. His retinal arterioles appeared normal. Psychophysical and electroretinographic test results for patient F1 were consistent with an early stage RP. We consider both patients C1 and F1 to have an early form of the typical RP displayed by their parents (C2 and F2, respectively).

Table 2. Summary of clinical findings.

Patient	Sex	Age	Visual acuity	Color error score	Night-blindness onset	ERG	EOG	Hearing	Dominant RP type
A1	F	13	20/30 20/25	16 11	Infancy	NR	1.3 1.5	Normal	1
B1	M	31	20/25 20/25	38 48	13 years	59 μV 59 μV	1.32 1.4	Normal	1
B2	M	33	20/20 20/20	15 12	13 years	NR	1.2 1.29	Normal	1
C1	F	25	20/15 20/15	38 26	3 years	59 μV 59 μV	1.53 1.46	Normal	1
C2	M	64	20/30 20/25	92 84	8 years	NR	1.31 1.45	Normal	1
D1	M	55	20/80 20/160	109 96	Infancy	NR NR	1.27 1.38	35 db loss at 1,000 Hz to 50 db loss 8,000 Hz	1
D2	M	47	20/50 10/200	140 210	Infancy	NR	1.08 1.18	55 db loss at 4,000 Hz (probable acoustic trauma)	1
D3	M	43	20/50 20/30	50 38	Infancy	NR NR	1.28 1.33	45 db loss at 4,000 Hz (probable acoustic trauma)	1
D4	M	39	20/60 20/60	64 113	Infancy	NR NR	1.34 1.33	70 db loss at 4,000 Hz	1
D5	F	35	20/60 20/60	70 56	Infancy	NR	--	Normal	1
D6	M	16	20/25 20/120	139 200	Infancy	NR	–	Normal	1
D7	F	14	20/30 20/40	88 60	Infancy	59 μV 71 μV	–	Normal	1

E1	F	11	20/30 20/40	19	Infancy	35 μV 24 μV	1.12 1.06	Normal	1
E2	M	45	20/20 20/80	77 166	Childhood	NR NR	1.4 1.45	40 db loss at 4,000 Hz	1
F1	M	8	20/30 20/30	124 136	No symptoms	82 μV 59 μV	–	Normal	1
F2	F	31	20/400 20/200	472 272	8 years	NR	1.23 1.28	Normal	1
G1	F	32	20/20 20/25	14 10	Early childhood	47 μV 59 μV	–	Normal	2
H1	F	29	20/20 20/16	60 34	19 years	94 μV 94 μV	1.17 1.18	Normal	2
I1	F	35	20/10 20/10	7 7	30 years	164 μV 178 μV	1.30 1.28	Normal	2
J1	F	54	20/20 20/25	108 56	40 years	NR	1.44 1.30	Normal	2
K1	M	48	20/25 20/20	122 142	43 years	NR	–	Normal	2
L1	M	31	20/40 20/40	90 160	18 years	44 μV 44 μV	–	Normal	2
M1	F	39	20/50 20/40	16 8	20 years	NR	1.23 1.27	Normal	2
M2	M	62	20/40 20/25	14 24	60 years	NR NR	–	40 db loss at 4,000 Hz & 8,000 Hz (probable acoustic trauma)	2
M3	F	59	20/60 20/60	222 243	40 years	NR NR	1.06 1.1	50 db loss at 4,000 Hz (probable acoustic trauma)	2

NR = nonrecordable.

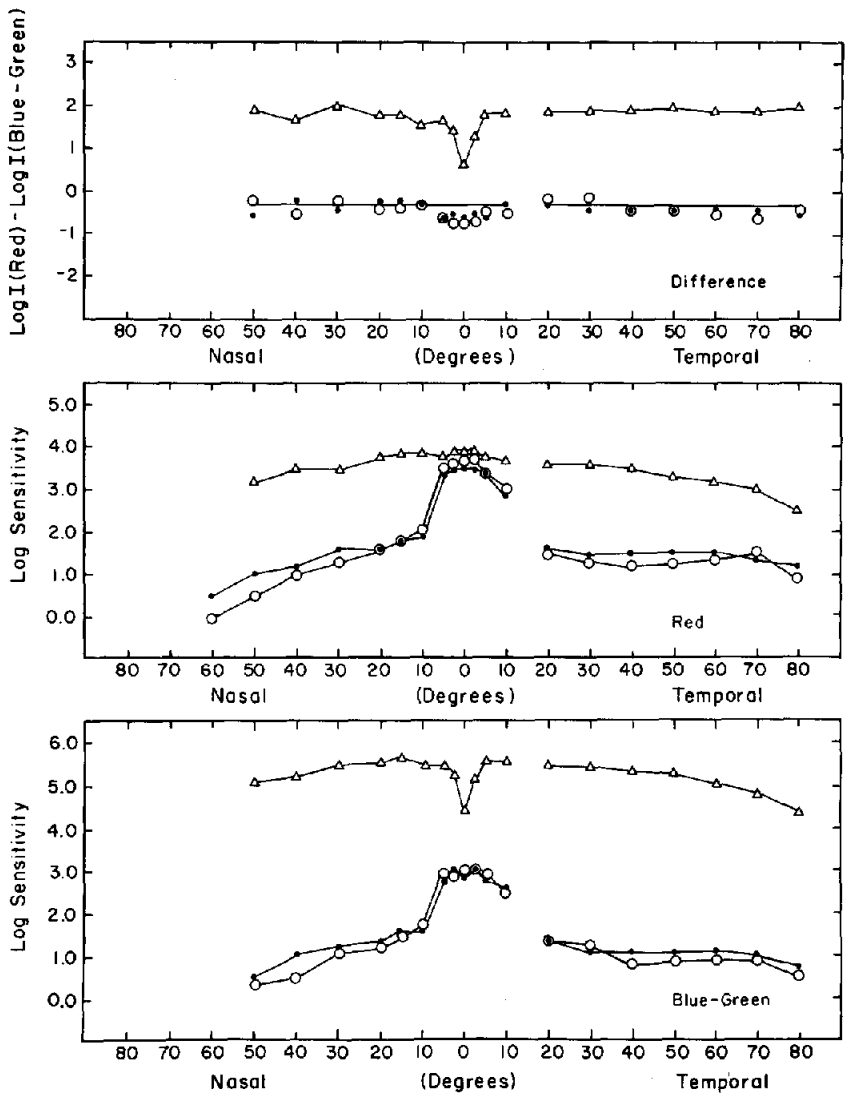

Figure 9. Log sensitivities at absolute threshold for the blue-green stimulus (bottom panel) and red stimulus (middle panel) are plotted for the right eye (filled circles) and left eye (open circles) of patient A1, as a function of retinal eccentricity along the horizontal meridian. Mean normal values determined in an earlier study (Massof & Finkelstein, 1979a) are plotted for comparison (open triangles). Differences between log threshold luminances for the red and blue-green stimuli are plotted as a function of retinal eccentricity along the horizontal meridian in the top panel (open circles and filled circles), along with mean normal values (open triangles). The solid line fit to the patient data is the prediction of the simulation model, assuming no rod contributions to absolute threshold (i.e., at least a 3.2 log unit reduction in rod sensitivity relative to cone sensitivity); thus, cones detected both stimuli everywhere in the visual field.

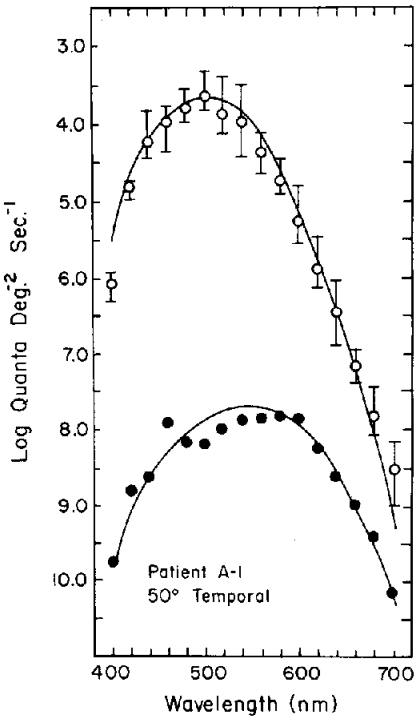

Figure 10. Absolute threshold spectral sensitivity measured at 50° temporal field in patient A1 (filled circles). The solid curve through the points is the normal cone spectral sensitivity function (C.I.E. photopic spectral sensitivity function corrected for the lack of macular pigment). The open circles with error bars are normal absolute-threshold spectral sensitivity values at the same retinal position. The solid curve fit to the open circles is the normal rod spectral sensitivity curve (C.I.E. scotopic spectral sensitivity function).

Dark adapted sensitivity profiles were obtained using the techniques outlined in the preceding methods section. On the basis of these measures, and the subsequent analyses, two sub-types of dominant RP were identified, type 1 characterized by an early and diffuse loss of rod sensitivity and type 2 characterized by a regionalized and combined loss of rod and cone sensitivity.

Dominant type 1: Early and diffuse loss of rod sensitivity

On the basis of absolute threshold profiles, this group of dominant RP patients has a diffuse loss of rod function with varying degrees of cone function loss. Initial rod sensitivity losses occurred in childhood, extensive cone function loss occurred later in the course of the disease. In this section, we describe data obtained from 16 RP patients in 6 pedigrees who represent this type of dominant RP.

Patient A1 is a 13 year-old girl. She reports being nightblind since infancy

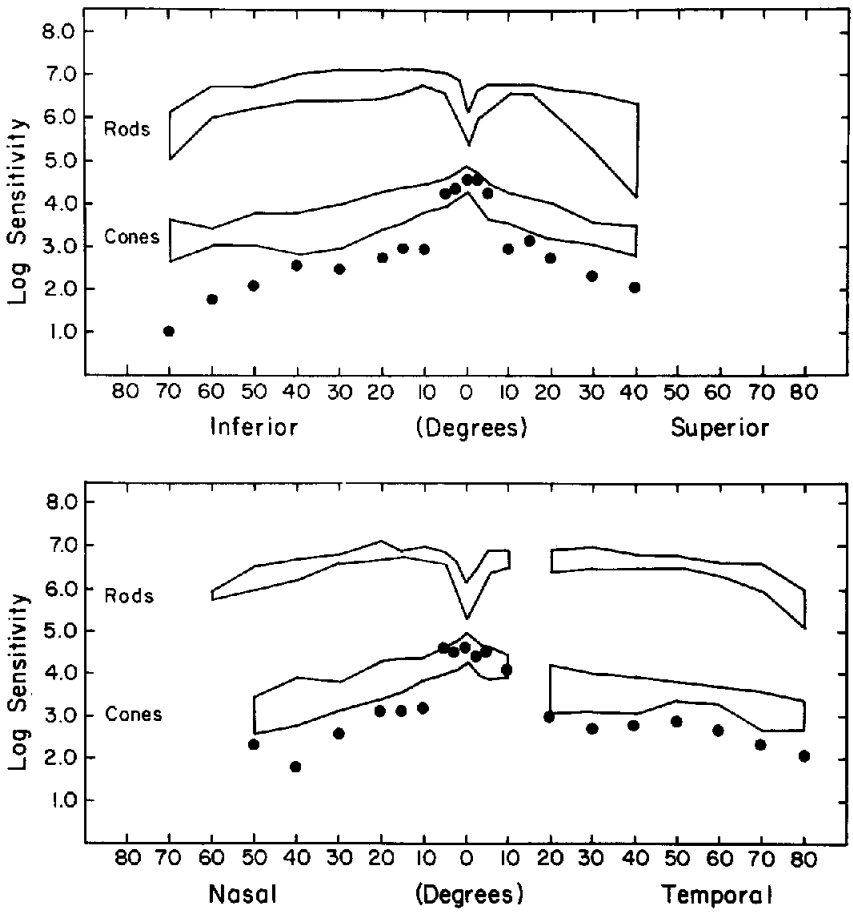

Figure 11. Cone sensitivities at absolute threshold for patient A1 (points) are plotted as a function of eccentricity along the horizontal meridian (lower panel) and vertical meridian (upper panel). The normal rod and cone ranges (from Figure 6) are plotted for comparison.

and has full visual fields (Fig. 8). The sensitivity profiles for her right eye have been reported previously (Massof & Finkelstein, 1979a); and as illustrated in the lower panel of Figure 9, sensitivity losses for the short-wavelength stimulus range from 1.5 log units at fixation to 4.5 log units in the periphery. As illustrated in the centre panel of Figure 9, sensitivities to the long-wavelength stimulus are nearly normal in the central 5° and fall to 2.5 log units below the normal mean in the periphery. The difference between log threshold luminances for the long-wavelength and short-wavelength stimuli is plotted as a function of eccentricity in the upper panel of Figure 9. The differences all

across the visual field are at the expected cone level of −0.3 log unit (solid line) plus-or-minus 0.3 log unit.

Because the log threshold luminance difference values in the upper panel of Figure 9 reflect cone spectral sensitivity at all retinal positions, cones alone detected both stimuli throughout the visual field. As a demonstration, Figure 10 illustrates the full absolute-threshold spectral sensitivity function, measured at 50° temporal field on this patient (Massof, Johnson & Finkelstein, 1981). These data are fit by the photopic spectral sensitivity curve, as would be predicted by the log threshold luminance difference value.

Patient A1 exhibits no evidence of rod function throughout the visual field. Because this patient has been nightblind since birth, we speculate that she may never have had functioning rods, or at least not since infancy.

To study the cone function of patient A1, we obtained absolute threshold profiles in the same manner as described in the methods section, but substituting a white light for the red or blue-green lights. Since we know from the data in Figure 9 that cones will mediate the detection of the white light at absolute threshold for patient A1, we can compare white light sensitivity profiles to the normal cone sensitivity profiles for the same white light plotted in Figure 4. These data, along with the normal cone sensitivity ranges, are plotted in Figure 11 for the horizontal (lower panel) and vertical meridians (upper panel). The patient's cone sensitivities are normal within 5° to 10° of fixation, falling .5 to 2 log units below the lower boundary of the normal range outside of this central zone. Thus, central cone function appears to be normal or nearly normal and peripheral cone function is reduced.

Figure 12 illustrates the data for two brothers from the second dominant RP pedigree (B). The patient represented by the open circles (B1) is 31 years old, has reported nightblindness since age 13, and has full visual fields with a narrow superior arcuate scotoma to the II/4 target at 15° to 20° from fixation (Fig. 8). This patient's brother (B2) is 33 years old with a similar clinical history. His visual fields are normal except for an encircling scotoma to the II/4 target at 10° to 20° from fixation (Fig. 8). The threshold data of patient B2 are represented by filled circles in Figure 12.

For both patients B1 and B2, sensitivities to the short-wavelength stimulus are reduced from 1 log unit at fixation to 4 log units in the periphery (see lower panel of Fig. 12). For the long-wavelength stimulus (center panel of Fig. 12), sensitivities are normal in the central 5° and fall to 2 log units below the normal mean in the periphery. There is a pronounced notch in the sensitivity profile at 15° nasal field for both stimuli. Like patient A1, the log threshold luminance difference profiles (upper panel of Fig. 12) for these two patients reflect cone spectral sensitivity for most retinal positions (−0.3 plus-or-minus 0.3 log unit).

The dashed line in the upper panel of Figure 12 illustrates the prediction by the simulation model of the difference profile if cones mediate detection at all retinal positions (rods reduced in sensitivity at least 3.2 log units more

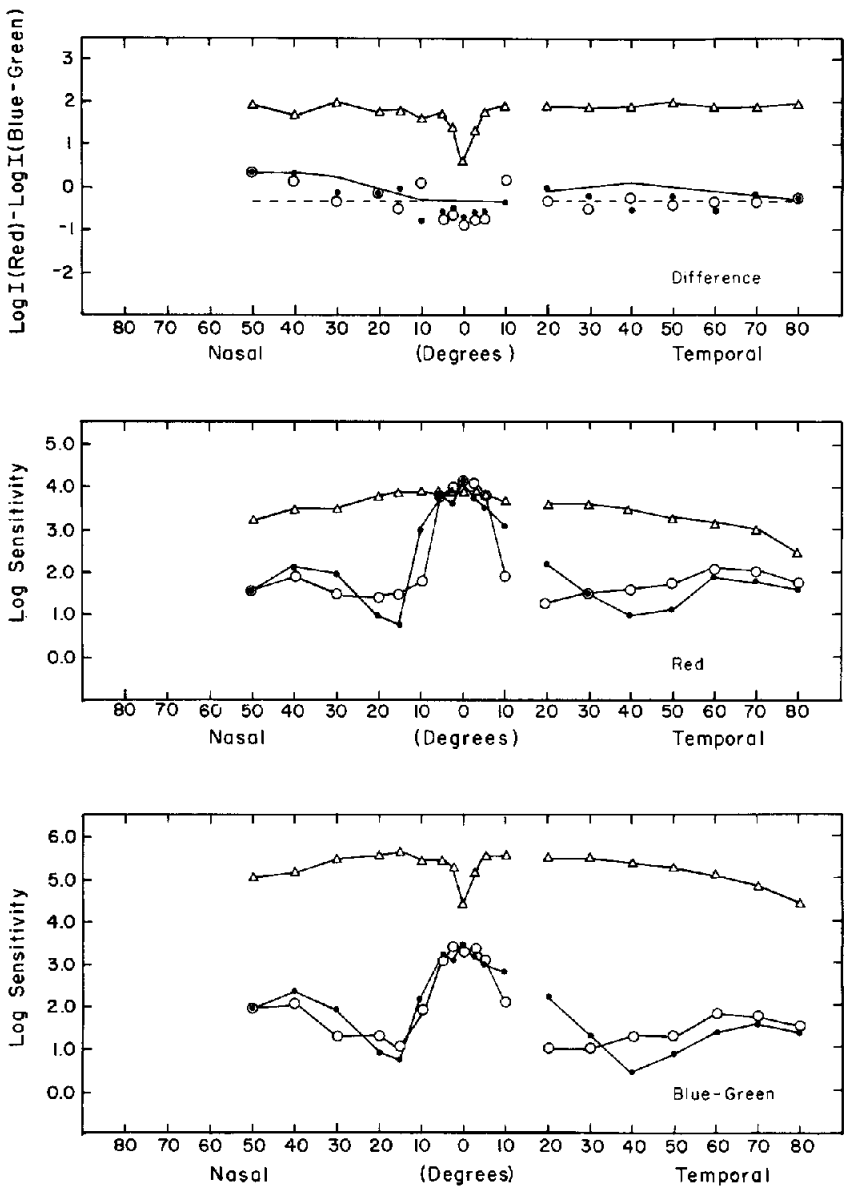

Figure 12. Same as Figure 9, but for patient B1 (open circles) and B2 (filled circles). The dashed line in the upper panel is the prediction of the simulation model, assuming no rod contributions to threshold (i.e. at least a 3.2 log unit reduction in rod sensitivity relative to cone sensitivity). The solid line in the upper panel is the prediction of the simulation model, assuming a 2.5 log unit reduction in rod sensitivity relative to cone sensitivity. That is, 2.5 was subtracted from each value in the second column of Table 1, and corresponding log threshold luminance difference values were generated from the function in Figure 3.

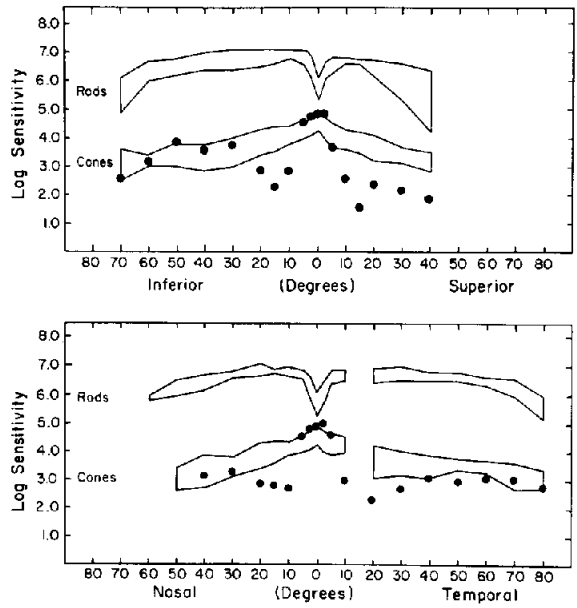

Figure 13. Same as Figure 11, but for patient B2.

than the cone sensitivity reduction). The fit by the simulation model can be improved for the nasal field if we assume that all the rods were reduced in sensitivity 2.5 log units more than the sensitivities of the cones were reduced (solid line in upper panel of Fig. 12). This latter prediction employs assumptions equivalent to those used to describe the normal increment thresholds on the 3.2 cd/m^2 green background (Fig. 6), using a 2.5 log unit rod reduction instead of the 2.2 log units used to explain the normal data.

Cone absolute threshold profiles for the white light were obtained for patient B2. As illustrated in Figure 13 for the horizontal (lower panel) and vertical meridians (upper panel), cone sensitivities fall within the normal range in the central 5° and again in the far periphery. In the area from 10° to 20° the cone sensitivities are 1 to 2 log units below the lower boundary of the normal range; this is the region of the encircling scotoma to the II/4 target.

For patients B1 and B2, we conclude that there was an early (at least by age 13) and diffuse loss of rod sensitivity, although not necessarily a total absence of rod function (from the suggestion of the simulation model). Cone sensitivity losses appear to be confined to an encircling band 10° to 20° from fixation. Central cone function is normal.

Data for the third dominant pedigree (C) are illustrated in Figure 14. The open circles represent the results for a 25-year-old woman (C1) who reported nightblindness onset occurring at age 3. Her visual fields are normal (Fig. 8). The triangles plotted in Figure 14 illustrate the results for patient C2, the

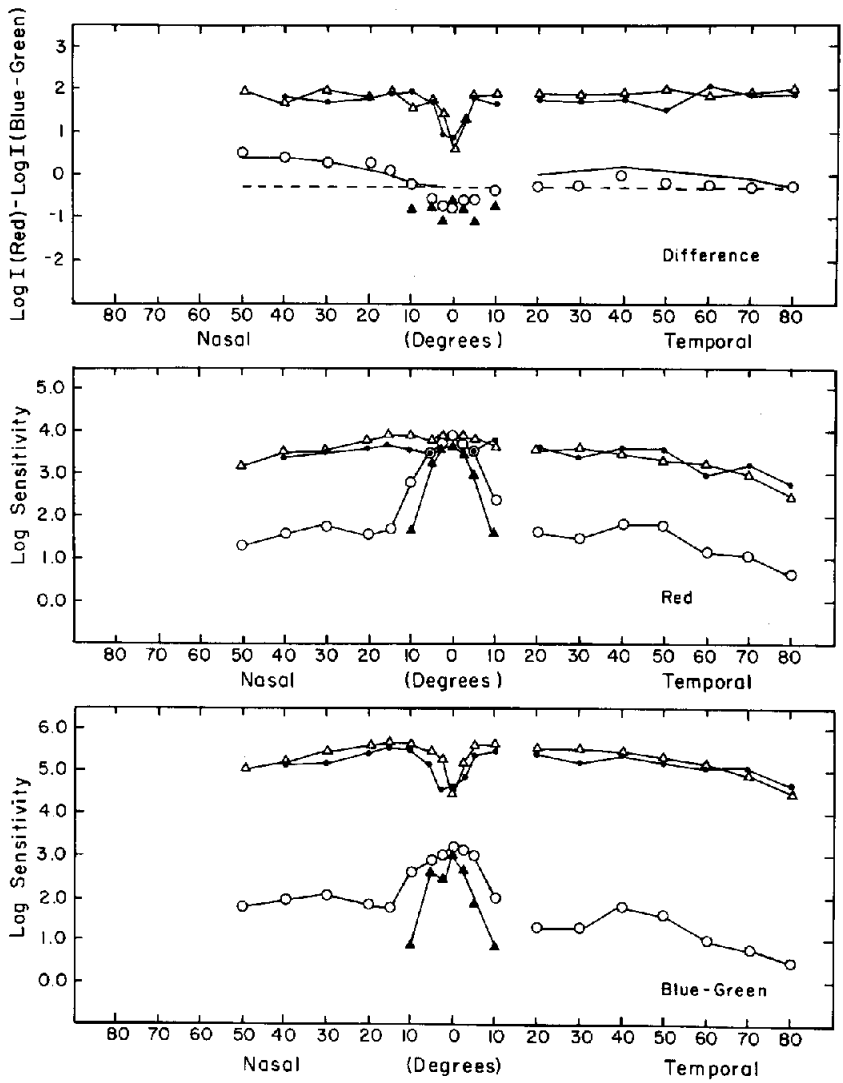

Figure 14. Same as Figure 9, but for patients C1 (open circles), C2 (filled triangles) and the unaffected sister of patient C1 (filled circles). The dashed line in the top panel is the prediction of the simulation model, assuming no rod contributions to the threshold (i.e., at least a 3.2 log unit reduction in rod sensitivity relative to cone sensitivity). The solid line in the top panel is the prediction of the simulation model, assuming a 2.5 log unit reduction in rod sensitivity relative to cone sensitivity.

64-year-old father of patient C1. He reported nightblindness onset occurred at age 8 and his visual fields are contracted to 15°, with an infero-temporal island of vision in the far periphery for the V/4 target, and contracted to 10° with no peripheral islands for the II/4 target (Fig. 8). The closed circles in

Figure 14 are the results for the 24-year-old sister of patient C1. She has neither signs nor symptoms of RP; and her data, which plot along the normal means, are included as an example of a normal family member.

As illustrated in the lower panel of Figure 14, sensitivity losses for the short-wavelength stimulus range from 1.3 log units at fixation to 4 log units in the periphery for patient C1 (open circles) and from 1.5 log units at fixation to 4.5 log units at 10° for patient C2 (filled triangles). No thresholds could be measured outside 10° for patient C2. For the long-wavelength stimulus (center panel of Fig. 14) sensitivities are normal for both patients in the central 5° and fall to 2 log units below the normal mean for patient C1 in the periphery and 2 log units below the normal mean at 10° for patient C2. Again, outside 20° no thresholds could be measured for patient C2. The log threshold luminance difference profiles are plotted in the upper panel of Figure 14. As for the other pedigrees, the differences are close to the cone determined value for much of the visual field.

If we assume complete absence of rod contributions to stimulus detection (i.e., rod sensitivity losses at least 3.2 log units greater than cone sensitivity losses), the simulation model predicts cone determined difference values for all positions in the visual field (dashed line in the upper panel of Fig. 14). Although this assumption can account for the data of patient C2, it does less well for patient C1. As for the preceding pedigree, the simulation model generates a better fit to the nasal data if we assume a 2.5 log unit greater sensitivity-loss for all rods than for cones (solid line).

Cone sensitivity profiles for patient C1 are plotted in Figure 15 for the horizontal (lower panel) and vertical meridians (upper panel). Cone sensitivities lie within the normal range in the central 5° and again peripheral to 30° nasally and inferiorly. Sensitivities are depressed by as much as 0.7 log unit below the lower boundary of the normal range for other field positions.

The description of patient C1 is similar to that of patients B1 and B2. In addition, we observe that cone sensitivities for patients C1 and C2 are identical and normal in the central 5°, despite the large discrepancy in visual field size for the two patients. Assuming patients C1 and C2 are following the same RP disease course, we might tentatively conclude that rod sensitivity is lost early and diffusely and cone sensitivities are progressively lost from the periphery towards the center, with the central 5° remaining relatively normal.

The patients in the fourth dominant pedigree (D) further illustrate trends supporting the type of natural history found for the patients in the third pedigree.

Patient D1 is a 55-year-old male, D2 is a 47-year-old male, D3 is a 43-year-old male, D4 is a 39-year-old male, D5 is a 35-year-old female, D6 is a 16-year-old male and D7 is a 14-year-old female. (Patients D1 through D5 are siblings; D6 is the son of D3, and D7 is the daughter of D4.) All of these patients report nightblindness since birth. Patients D1 and D2 have 15° fields for the V/4 target and 10° fields for the II/4 target. Patients D3, D4 and D5

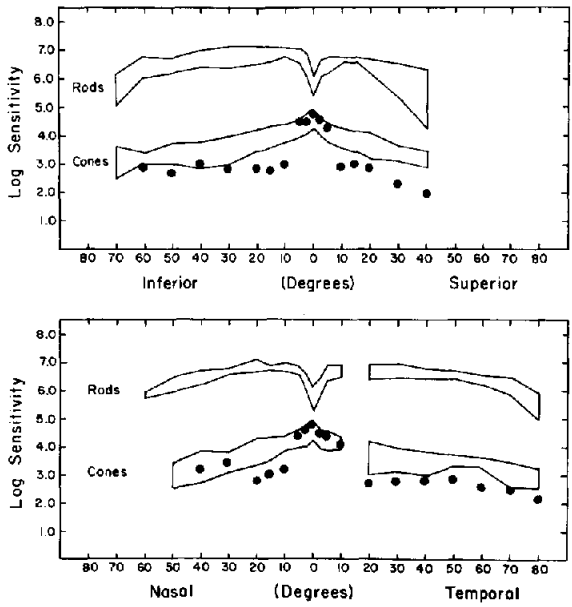

Figure 15. Same as Figure 11, but for patient C1.

have 20° to 25° fields with a temporal visual island for the V/4 target, and 15° to 20° fields for the II/4 target. Patients D6 and D7 have full fields for the V/4 target and 35° to 40° fields for the II/4 target (Fig. 8).

Figure 16 illustrates the sensitivity profiles for the older patients in this pedigree (D1 through D5). As shown in the lower panel of Figure 16, sensitivity losses range from 1.5 to 2.3 log units at fixation, to greater than 4.5 log units at 10° for the short-wavelength stimulus. The sensitivity profiles for these five patients are remarkably similar; no threshold measures could be obtained on any of the patients outside 15° (except for one point at 20° temporal for patient D3). For the long wavelength stimulus (center panel of Fig. 16) sensitivity losses range from 0.8 to 1.3 log units at fixation to greater than 2.5 log units at 10°. Again, no threshold measures could be obtained in the peripheral field. The log threshold luminance difference profiles are plotted in upper panel of Figure 16. All values plot close to the cone determined level of −0.3. The solid line represents the prediction of the simulation model, assuming no rod contributions to detection.

Figure 17 illustrates the sensitivity profiles for the two younger patients in this pedigree (D6 and D7). For the short-wavelength stimulus (lower panel of Fig. 17), sensitivity losses range from 1.8 log units at fixation to over 4.5 log units in the periphery. For the long-wavelength stimulus (center panel of Fig. 17) sensitivity losses range from 0.4 log units at fixation to over 3 log units in the periphery. For both the short and long-wavelength stimuli

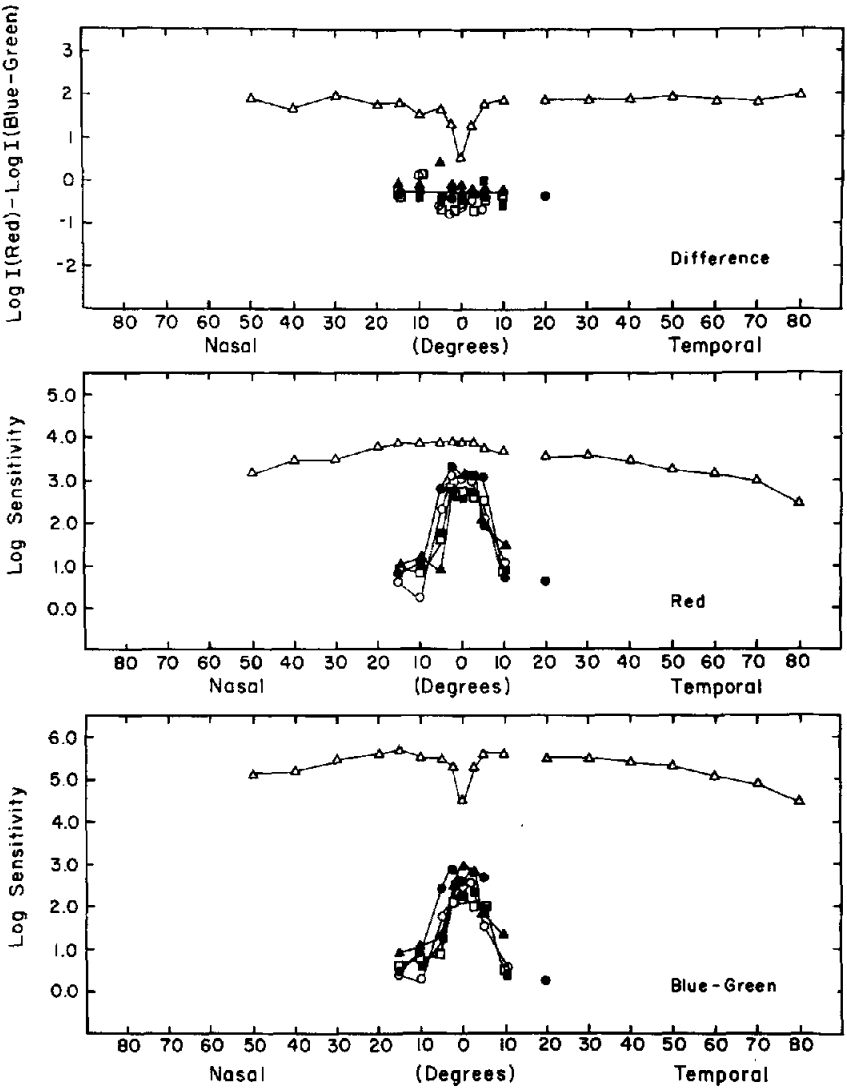

Figure 16. Same as Figure 9, but for patients D1 (open square), D2 (open circle), D3 (filled triangle), D4 (filled square), and D5 (filled circle). The solid line in the upper panel is the prediction of the simulation model, assuming no rod contributions to threshold.

these two patients have similar, but not identical, sensitivity profiles. There is, however, a high degree of similarity between their log threshold luminance difference profiles (upper panel of Fig. 17). This greater concordance indicates the two patients have the same spectral sensitivities, despite absolute threshold differences. The difference values are close to the cone determined level of

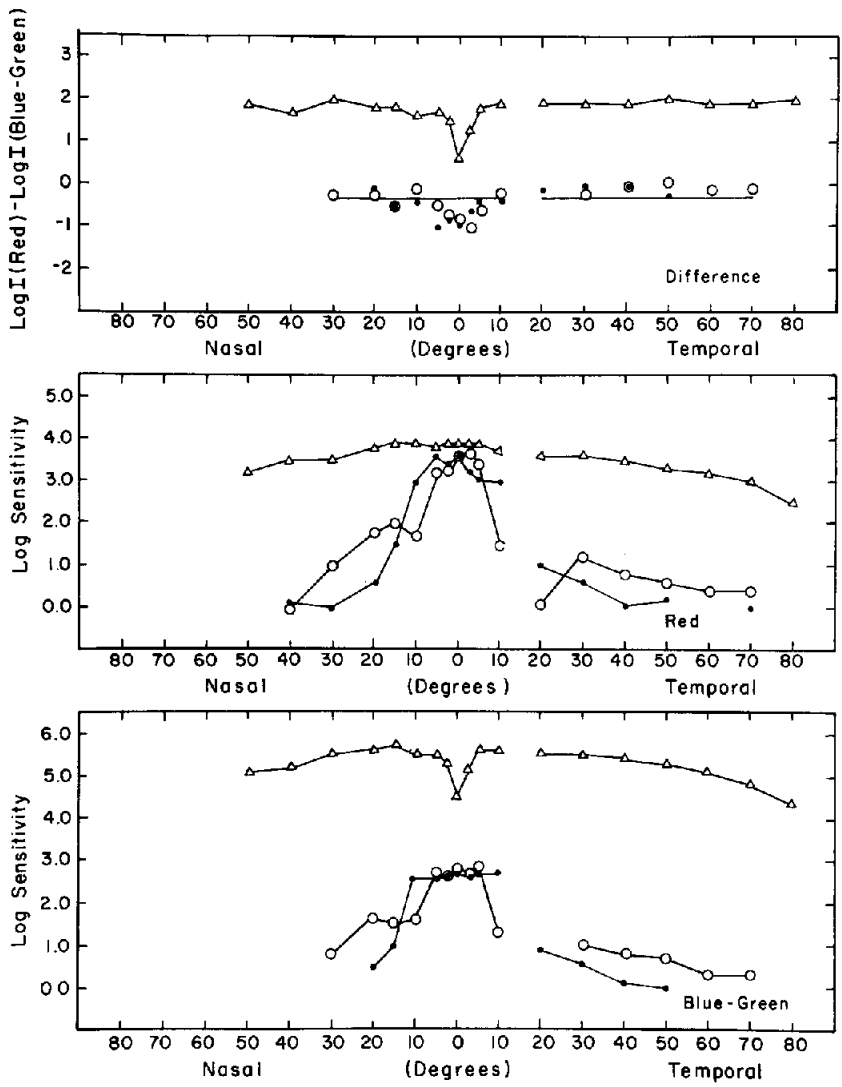

Figure 17. Same as Figure 9, but for patients D6 (filled circles) and D7 (open circles). Solid line fit to the patient data in the upper panel is the prediction of the simulation model, assuming no rod contributions to threshold (i.e., at least a 3.2 log unit reduction in rod sensitivity relative to cone sensitivity).

−0.3, and the assumption of no rod contributions to stimulus detection generates the best fit from the simulation model (solid line in the top panel of Fig. 17). Difference values less than −0.3, as for fixation in these patients, also indicate cone spectral sensitivity, but shifted toward longer wavelengths.

Comparisons of Figures 16 and 17 illustrate an obvious difference in field

size between the young and older patients, but surprisingly no difference among the older patients (Fig. 16). There appears to be a loss in visual field in this pedigree that must occur prior to age 35. The field loss then seems to level off to retention within about 10°.

The next patients, in the fifth and sixth autosomal dominant pedigrees, originally were included in a third class of threshold patterns (Massof & Finkelstein, 1979a); that is, superficially the log threshold luminance difference profiles suggested that rod sensitivity losses preceded cone sensitivity losses, with variations in the rod to cone sensitivity relations across the visual field. As will be seen, however, the application of the simulation model indicates that these patients probably belong in the same RP subclass as the first four pedigrees of the present study.

From the fifth dominant pedigree (E), patient E1 is an 11-year-old girl who has been nightblind since birth. Her fields are normal for the V/4 target and contracted to 45° for the II/4 target (Fig. 8). Patient E2 is the 45-year-old father of E1. He reports nightblindness since childhood. His visual fields are contracted to 20° for the V/4 target and 10° for the II/4 target (Fig. 8).

Figure 18 illustrates the sensitivity profiles obtained on patients E1 and E2 for the short-wavelength stimulus (lower panel) and for the long-wavelength stimulus (center panel). For patient E1 (closed circles), sensitivity losses ranged from 1.5 log units at fixation to 4.5 log units in the periphery for the short-wavelength stimulus (lower panel). Thresholds could not be measured from 30° to 40° nasal nor beyond 50° temporal. For the long-wavelength stimulus (center panel) sensitivities were normal in the central 10° and fell to 3 log units below the normal mean in the periphery. Again, thresholds could not be measured at eccentricities beyond 20° nasal and 50° temporal. Sensitivity losses for patient E2 (open circles) ranged from 2.2 log units at fixation to 5.2 log units at 10° nasal for the short-wavelength stimulus (lower panel), and from 1.2 log units at fixation to 3.4 log units at 10° nasal for the long-wavelength stimulus (center panel). No thresholds could be measured outside of 10° for either stimulus.

The log threshold luminance difference profiles for patients E1 and E2 are illustrated in the upper panel of Figure 18. For patient E1 (closed circles), the difference values are at the cone level in the central 10° and ascend toward the rod level in the periphery. The difference values for E2 (open circles) are close to the cone level for all measured positions. The dashed line is the prediction of the simulation model if there were no rod contributions to thresholds. This prediction obviously is invalid outside the central 10°. In contrast, if we assume that the thresholds of all the retinal rods were evaluated only 2 log units more than the elevation of cone thresholds, the simulation model generates an excellent fit to the data (solid line).

The pattern just described for the fifth dominant pedigree also is seen in the sixth possibly-dominant pedigree (F). Patient F1 is an 8-year-old boy. He has no complaints of nightblindness and his visual fields are normal for the

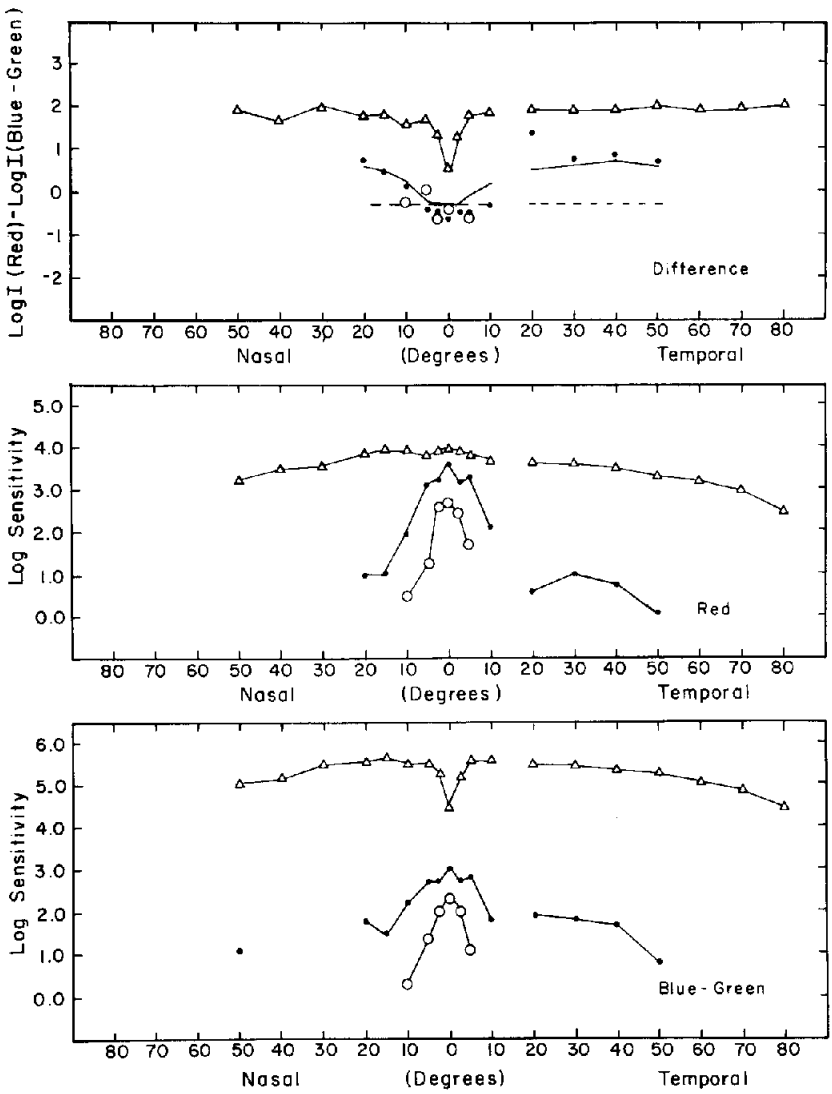

Figure 18. Same as Figure 9, but for patients E1 (filled circles) and E2 (open circles). The dashed line in the upper panel is the prediction of the simulation model, assuming no rod contributions to threshold (at least a 3.2 log reduction in rod sensitivity relative to cone sensitivity). The solid line in the upper panel is the prediction of the simulation model, assuming a 2.0 log unit reduction in rod sensitivity relative to cone sensitivity. That is, 2.0 was subtracted from every value in the second column of Table 1, and new log luminance difference thresholds were computed from the function in Figure 3.

V/4 and II/4 targets (Fig. 8). Patient F2 is the 31-year-old mother of F1. She reports nightblindness onset occurred at about age 8; her visual fields are contracted to 30° for the V/4 target and 10° for the II/4 target (Fig. 8).

Sensitivity profiles for patients F1 and F2 are illustrated in Figure 19.

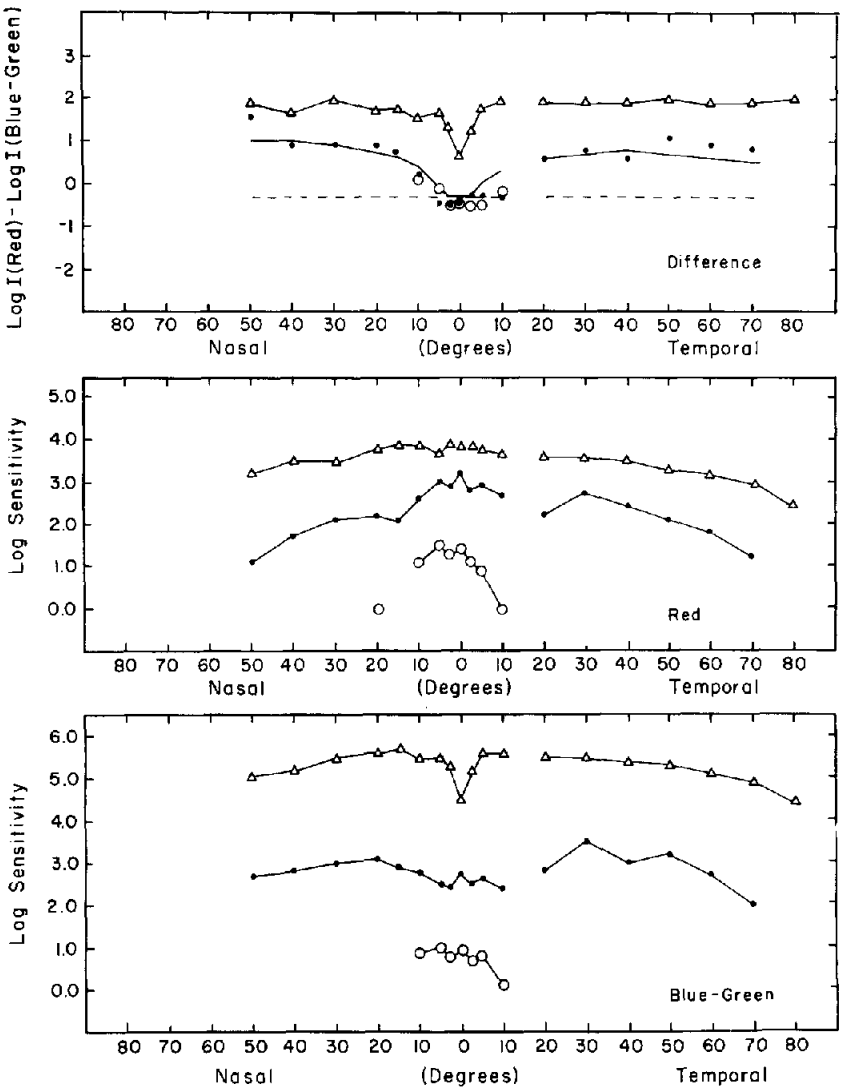

Figure 19. Same as Figure 9, but for patients F1 (filled circles) and F2 (open circles). The dashed line in the top panel is the prediction of the simulation model, assuming no rod contributions to threshold. The solid line in the top panel is the prediction of the simulation model, assuming rod sensitivity is depressed two log units more than cone sensitivity, i.e., 2.0 was subtracted from each value of the second column of Table 1, and new luminance difference thresholds were computed from the function in Figure 3.

Patient F1 (closed circles) has sensitivity losses ranging from 1.7 log units at fixation to 2.8 log units in the periphery for the short-wavelength target (lower panel). For the long-wavelength stimulus (center panel) sensitivities are close to normal near fixation and fall to 2.1 log units below the normal mean

in the periphery. For patient F2 (open circles) sensitivities could be measured only in the central 10° for both the short and long-wavelength stimuli (with the exception of a point at 20° nasal for the long-wavelength stimulus). Sensitivity depressions ranged from 3.6 log units at fixation to 5.5 log units at 10° for the short-wavelength stimulus (lower panel) and from 2.5 log units at fixation to 3.6 log units at 10° for the long-wavelength stimulus (center panel).

The absolute threshold log luminance difference profiles are plotted for patients F1 and F2 in the upper panel of Figure 19. As was seen for patient E1 (Fig. 17), difference values for patient F1 (closed circles) are at the cone determined level in the central 10° and ascend toward the rod level in the periphery.

Figure 20 illustrates absolute threshold spectral sensitivity data from an earlier study (Massof, Johnson & Finkelstein, 1981) at 30° temporal on patient F1; short-wavelength sensitivities fit the standard scotopic visibility curve, and long-wavelength sensitivities fit the standard photopic visibility curve. This combination of rod and cone contributions to absolute thresholds accounts for the difference values in the upper panel of Figure 19 that are intermediate – that is, between the rod and cone levels.

The dashed line in the upper panel of Figure 19 is the prediction of the simulation model if there are no rod contributions to stimulus detection. This prediction obviously does not describe the data outside of 10°. The solid line is the prediction of the simulation model if we assume that all the rods were reduced in sensitivity 2 log units more than the sensitivity reduction of the cones. This latter assumption generates an excellent description of the data from the simulation model.

Comments. For the six dominant pedigrees (16 patients) described here as belonging to type 1, the patient history and the application of the simulation model suggest that all in this group may be characterized as showing an early and diffuse loss of rod sensitivity. Patients A1, D6 and D7 had no evidence of rod function. According to the simulation model, rod function would not be measured if all the retinal rods were reduced in sensitivity at least 3.2 log units more than the cone sensitivities were reduced. Patients B1, B2 and C1 had difference threshold profiles suggesting a small rod intrusion in the periphery. Their data were best described by the simulation model when we assumed that all the rods were reduced in sensitivity 2.5 log units more than the reduction in cone sensitivity. Patients E1 and F1 had cone determined thresholds in the central 10° and significant rod contributions in the periphery. Their data could be accounted for by the simulation model if we assumed a degree of sensitivity loss of all the rods that was 2 log units greater than the sensitivity loss of the cones. Thus, the simulation model suggests that all these patients have the same disease mechanism, viz., a diffuse and uniform reduction in rod sensitivity, but they vary in the magnitude of rod sensitivity loss relative to cone sensitivity loss.

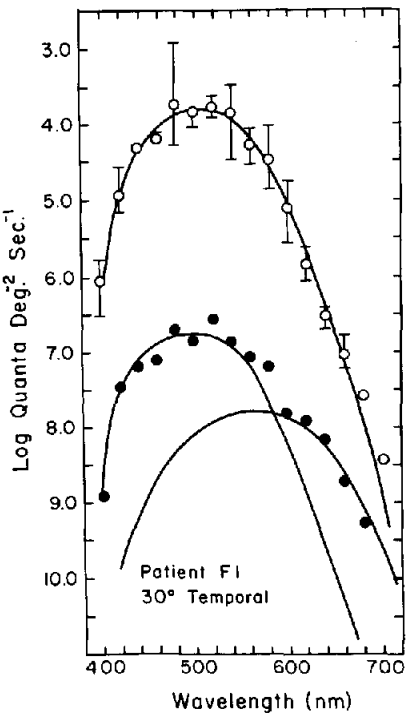

Figure 20. Same as Figure 10, but for patient F1 at 30° temporal field (filled circles). The solid curves fit to the patient data are the normal rod function (far-left-most curve) and normal cone function (far-right-most curve). The open circles and error bars are the normal spectral sensitivities for this eccentricity. The solid curve fit to the normal data is the normal rod function.

From the data of the younger patients and from the reports of childhood onset of nightblindness, the putative diffuse rod-sensitivity loss must occur very early, perhaps even congenitally. From the data on older patients, there obviously is a progressive loss of cone function. For patients E1 and F1, in particular, we may be observing a rod function loss in progress which may pass through stages (such as those seen in patients B1, B2 and C1) to a stage at which there are no rod contributions to stimulus detection, as in patient A1. From comparisons of ages, it is clear that such progression, if it exists, must vary considerably among pedigrees.

An alternative explanation is that the stage is set early in life as to the initial degree of rod function loss; then disease progression could be a combined loss of both cone function and the remaining rod function. This mechanism would preserve the initial absolute threshold log luminance difference value, despite continued losses of dark-adapted sensitivity.

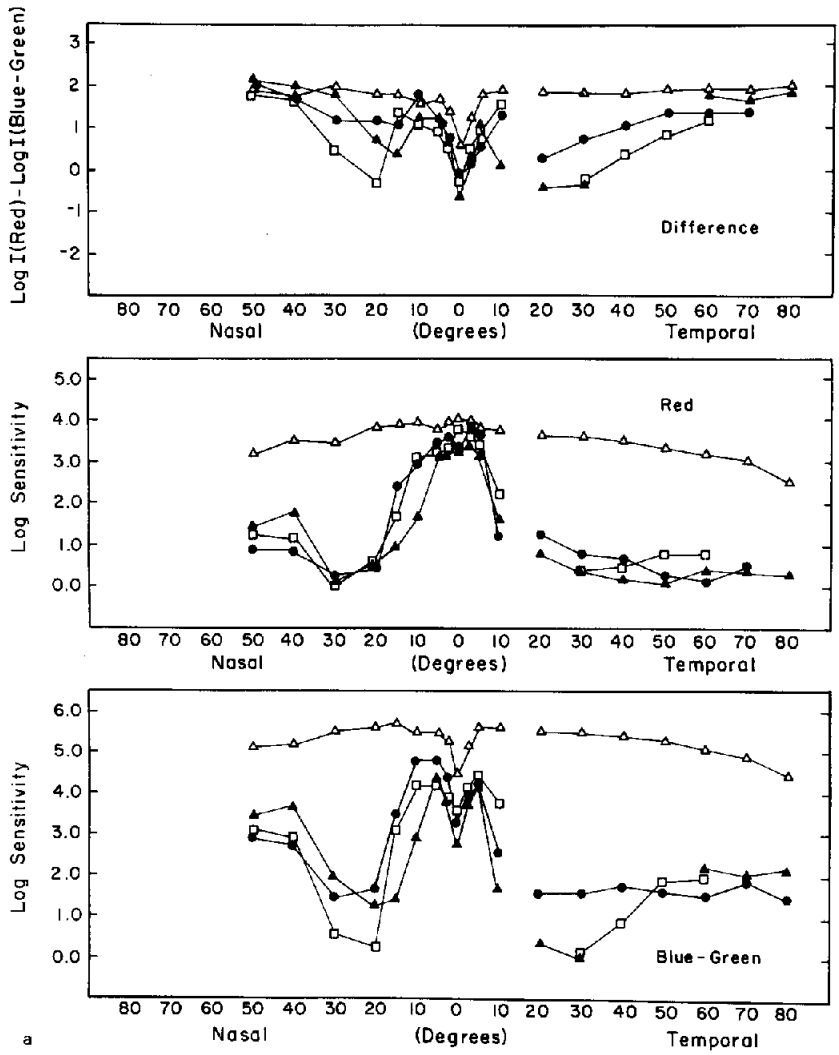

Dominant type 2: Regionalized and combined loss of rod and cone sensitivity

In our evaluation of dominant RP patients we have observed a pattern in threshold profiles for some pedigrees that defined a grouping separate from the previously described type 1. The patients in the second group, type 2, appear to have later onset of nightblindness, less-severe initial sensitivity losses, and threshold elevations that suggest a combined loss of rod and cone sensitivities that follow a regionalized pattern in the fundus.

Patient G1, from the seventh dominant pedigree, is a 32-year-old woman.

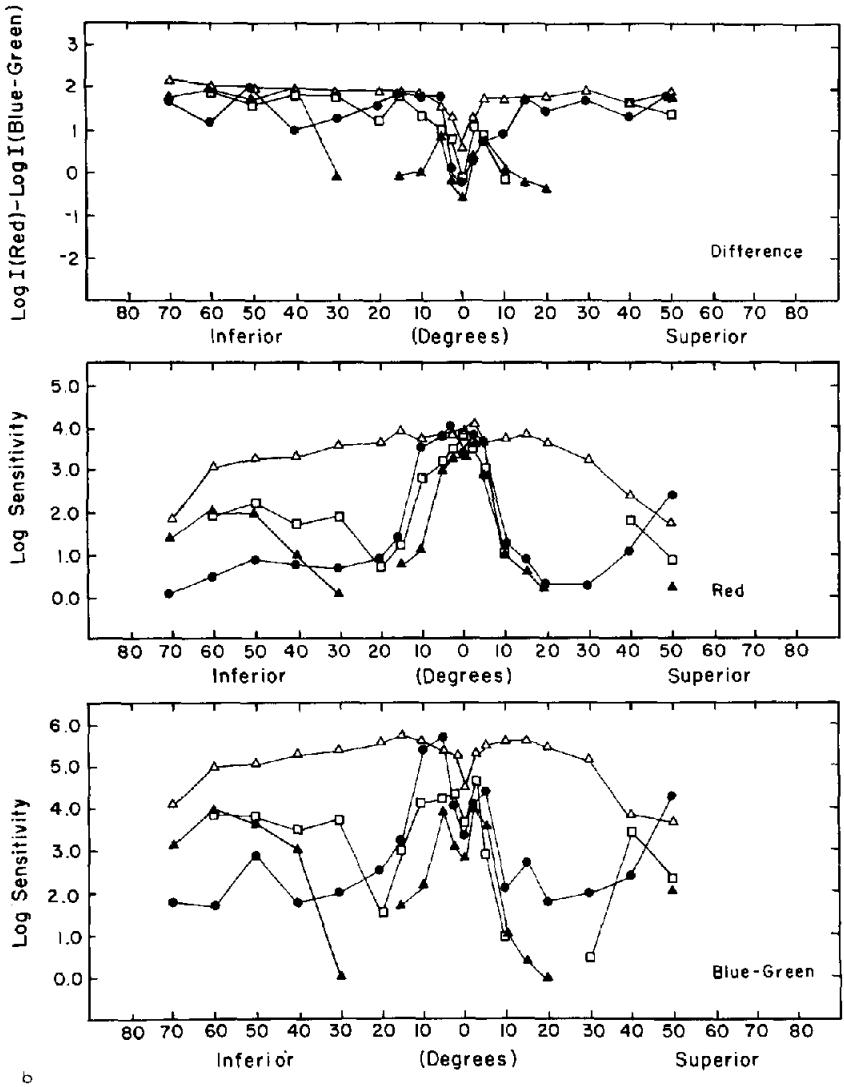

Figure 21. Same as Figure 9, but for patients G1 (filled circles), H1 (filled triangles), and I1 (open squares). Profiles are plotted for the horizontal meridian (a) and vertical meridian (b).

She reports nightblindness onset occurring in early childhood. Her visual fields are normal of the V/4 target, and there are partial mid-peripheral ring scotomas for the II/4 target (Fig. 8). Patient H1, from the eighth dominant pedigree, is a 29-year-old woman. She reports nightblindness onset noticed at age 19. Her visual fields are normal for the V/4 and II/4 targets (Fig. 8). From the ninth dominant pedigree, patient I1 is a 35-year-old-woman. She reports

nightblindness onset at age 30, and she has visual fields normal to the V/4 and II/4 targets, with the exception of partial encircling scotomas 15° to 30° from fixation, mainly in the superior field (Fig. 8).

The sensitivity profiles for patients G1, H1 and I1 are plotted together for the horizontal meridian in Figure 21a, and for the vertical meridian in Figure 21b. Sensitivity losses at fixation are 1.2 log units for G1 (closed circles), 1.7 log units for H1 (closed triangles), and 0.9 log units for I1 (open squares) for the short-wavelength stimulus (lower panels); and, for all three patients, sensitivity measures are within 0.5 log units of the normal mean for the long-wavelength stimulus (center panels). Sensitivities plunge to between 4 and 5 log units below the normal mean in a mid-peripheral band (15° to 40° from fixation) for the short-wavelength stimulus (lower panels) and fall 3 log units in the same zone for the long-wavelength stimulus (center panels). Although these patients are from three different dominant pedigrees, their sensitivity profiles are remarkably similar.

The absolute threshold log luminance difference profiles are illustrated in the upper panels of Figures 21a and 21b. Except for the mid-peripheral band, the difference values are near the normal rod levels; this occurs despite threshold elevations as great as 2 log units. (Because of the intermediate difference values in the mid-periphery, patient I1 previously was assigned to Group 3 (see Massof & Finkelstein, 1979a). However, because of her similarity to the other patients, coupled with her data for the vertical meridian, we believe she belongs in the type 2 subgroup of dominant RP.) No uniform manipulations of rod sensitivity in the simulation model can generate a prediction that approximates the difference value profiles of these patients.

The two important features of the data in Figures 21a and 21b are: (1) the regional differences in sensitivity losses and (2) the retention of rod-level difference values in the periphery despite 2 log unit threshold elevations. Figure 22 illustrates absolute threshold spectral sensitivity for patient I1 at 40° nasal; even with 2 log unit threshold elevations, her data are well-described by the normal scotopic spectral sensitivity curve.

The next sampling of type 2 patients to be described, representing three additional dominant pedigrees, appear to have more-advanced RP in terms of field loss than the preceding three patients.

Patient J1 is a 54-year-old female from the tenth dominant pedigree. She reported nightblindness onset occurring at age 40. Her peripheral visual field is normal and she has a mid-peripheral ring-scotoma to the V/4 target; for the II/4 target, her fields are contracted to 15° (Fig. 8). Patient K1 is a 48-year-old male from the eleventh dominant pedigree. He reports that nightblindness onset occurred at age 43. Using the V/4 target, his peripheral visual fields are of normal extent with a mid-peripheral ring scotoma extending from 10° temporal to 60° temporal; on the nasal side the scotoma borders range from 10° to 15°. With the II/4 target, his fields are contracted to 15° with far peripheral islands of vision retained (Fig. 8). Patient L1 is a 31-year-old male from the

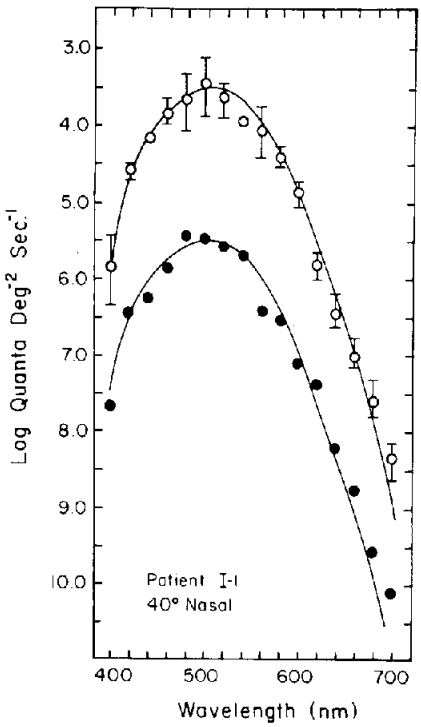

Figure 22. Same as Figure 10, but for patient I1 at 40° nasal field (filled circles). The solid curve fit to the patient data is the normal rod spectral sensitivity function. The normal data (open circles and error bars) for the same field position are also fit by the normal rod spectral sensitivity function (solid curve).

twelfth dominant pedigree. He reports childhood onset of nightblindness. Visual fields are full, with a partial temporal ring scotoma broken through superiorly with the V/4 target; with the II/4 target, fields are contracted to 10° (Fig. 8).

The sensitivity profiles for the horizontal meridian of patients J1, K1 and L1 are plotted together in Figure 23. Sensitivity losses range from 1.5 log units at fixation to 4.0 log units in the periphery for the short-wavelength stimulus (lower panel of Fig. 23). Thresholds were not measurable in the mid-peripheral field, the region of the ring scotoma; similar sensitivity losses occur for the long-wavelength stimulus (center panel of Fig. 23), with foveal sensitivities normal for patient J1 and K1 and depressed 1.5 log units for patient L1.

The absolute threshold log luminance difference profiles are plotted in the upper panel of Figure 23. As was seen for the three preceding patients (Fig. 21), cone determined values are present at fixation (with the exception of patient L1 who has an intermediate value) and rod determined values are present in the far periphery. The rod levels are obtained even with sensitivity

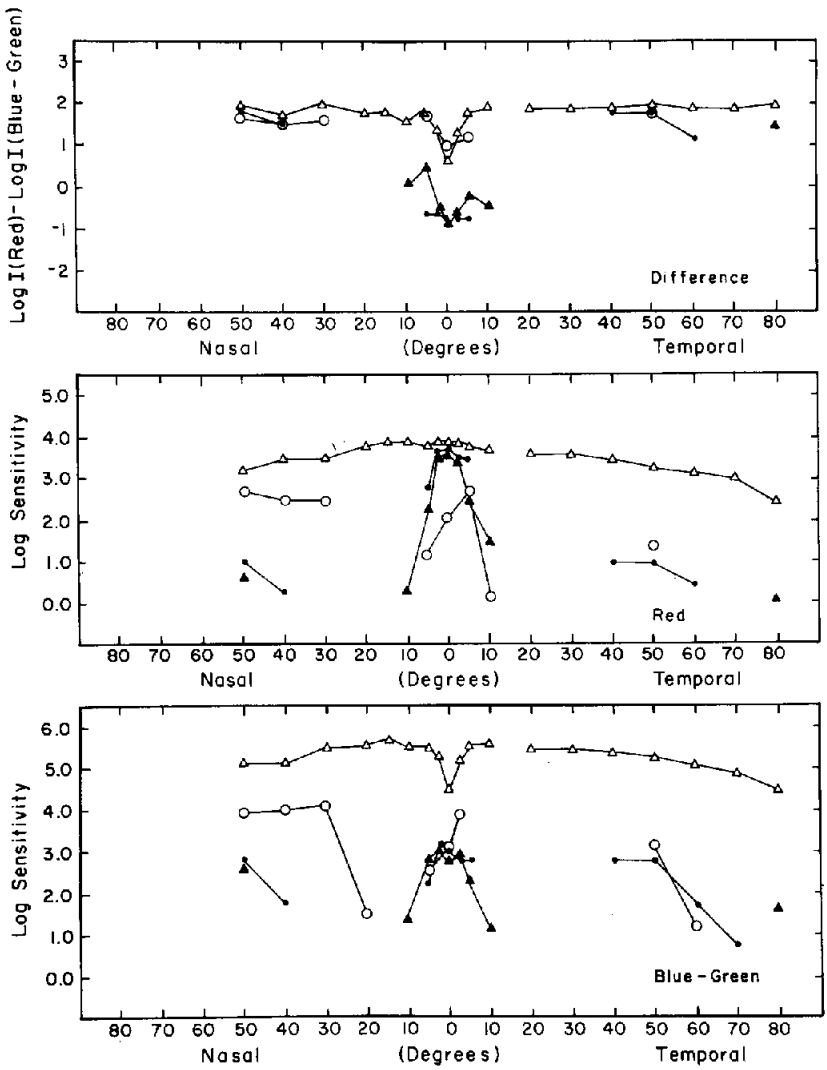

Figure 23. Same as Figure 9, but for patients J1 (filled triangles), K1 (filled circles), and L1 (open circles).

losses as great as 3 log units. Thus, as discussed earlier, there must be concomitant losses of rod and cone sensitivity.

The sensitivity and log threshold luminance difference profiles for patients J1, K1 and L1 (Fig. 23) are quite similar to the profiles of patients G1, H1 and I1 (Fig. 21a). As shown in Figure 24, the main differences are greater sensitivity losses from 2.5° to 10° for patients J1, K1 and L1, and the presence of a ring scotoma for these patients where there are prominent sensitivity

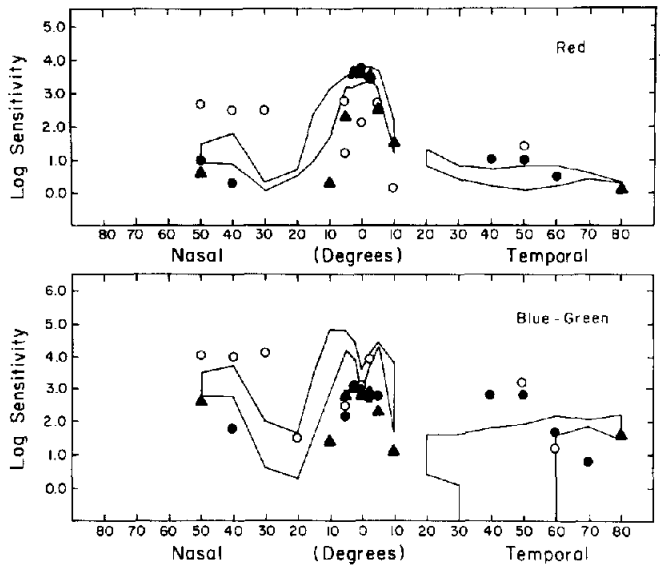

Figure 24. Log sensitivity profiles for patients J1 (filled triangles), K1 (filled circles), L1 (open circles) (replotted from Figure 23) are compared to the range of sensitivities for patients G1, H1, and I1 (cf. Fig. 21a).

depressions in the profiles of patients G1, H1, I1. These two groups of patients may be thought of as manifesting different stages of the same disease; it appears that the progression of sensitivity loss occurs mainly in the near and mid-periphery. In addition, when the sensitivity depressions become large (e.g., about 3 log units for the long-wavelength stimulus) the log luminance difference values begin to favor cones. This latter observation is especially evident in comparing short-wavelength sensitivity and log luminance difference values for patients G1, H1 and I1 at 20° nasal (Fig. 21a). No uniform manipulation of rod sensitivity relative to cone sensitivity will yield satisfactory predictions from the simulation model.

The final group of type 2 patients is from the thirteenth dominant pedigree; and their sensitivity profiles are the most ambiguous. Nevertheless, it appears that these patients represent the same disease process that has been described for type 2, and that they are still more advanced in sensitivity loss.

Patient M1 is a 39-year-old female. She reports nightblindness occurring at age 20. Using the V/4 target, her peripheral visual fields are full, with narrow mid-peripheral ring scotomas. Using the II/4 target, her fields are contracted to 20° with peripheral islands of vision retained (see Fig. 8). Patient M2 is a 62-year-old male, the father of patient M1. He reports that nightblindness onset began at age 60. Using the V/4 target, his visual fields are contracted to 20° with large temporal islands of vision. Using the II/4 target, visual fields are contracted to 15° with no peripheral islands (see Fig. 8). Patient M3 is a

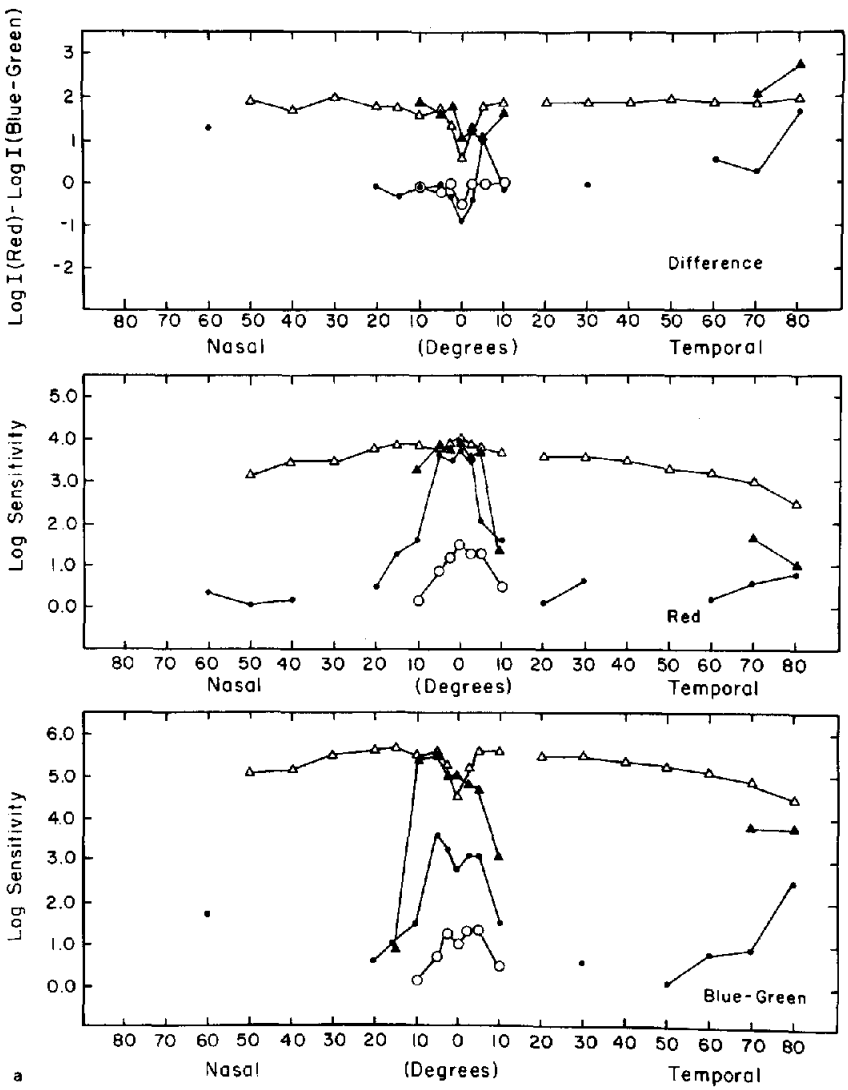

59-year-old female who is the sister of patient M2. She reports nightblindness onset beginning at age 30. Her visual fields are nearly identical to those of patient M2 (see Fig. 8).

Absolute threshold profiles for patients M1, M2 and M3 are plotted together in Figure 25 for the horizontal meridian (Fig. 25a) and for the vertical meridian (Fig. 25b). Patient M1 (closed circles) has sensitivity depressions for the short-wavelength stimulus, ranging from 1.7 log units at fixation to 5.5 log units in the periphery. Sensitivities to the long-wavelength stimulus are normal in the central field, falling to over 3 log units below the

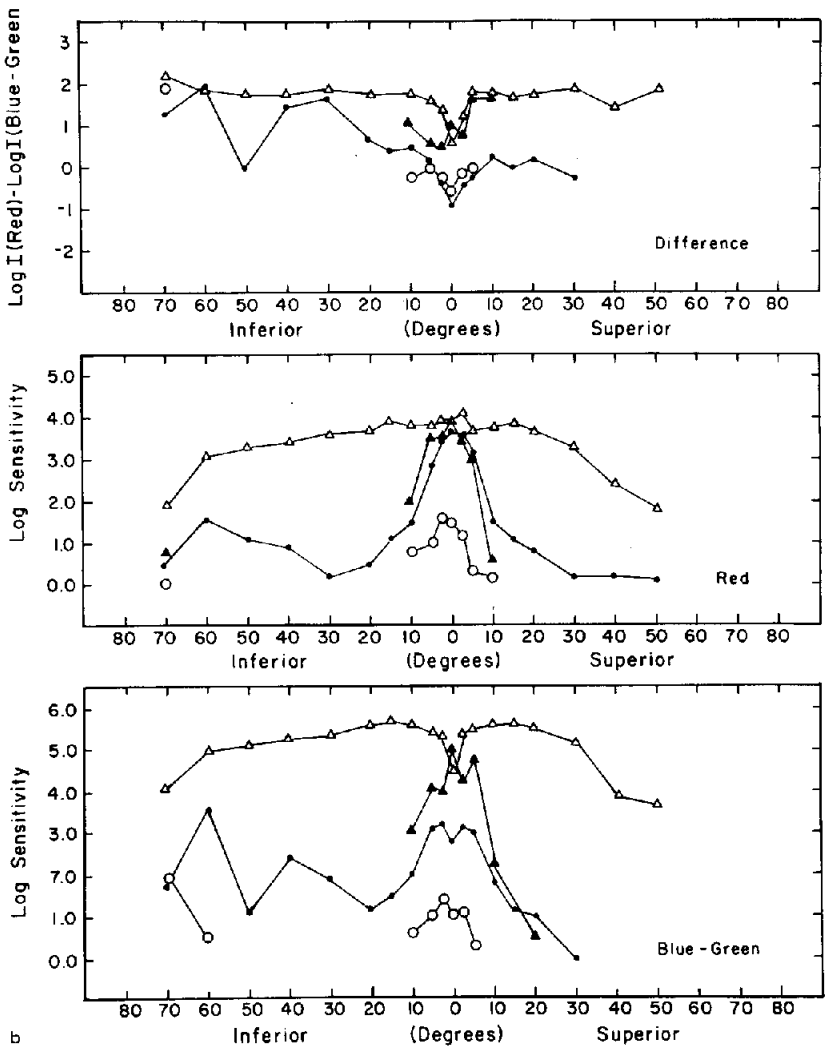

Figure 25. Same as Figure 9 but for patients M1 (filled circles), M2 (filled triangles), and M3 (open circles) along the horizontal (a) and vertical (b) meridians.

normal mean in the periphery. Sensitivities could not be measured in the mid-peripheral zone along the horizontal meridian for either stimulus. Log threshold luminance difference values (upper panels of Figs. 25a and b) are at the cone level in the central field, ascending to rod levels in the periphery, with the exception of 5° temporal, which is an intermediate value.

Patient M2 (filled triangles) has normal sensitivities and difference values in the central field. By 10° to 20° in all directions, the sensitivities plunge to non-measurable values. Sensitivities are measurable again in the far temporal

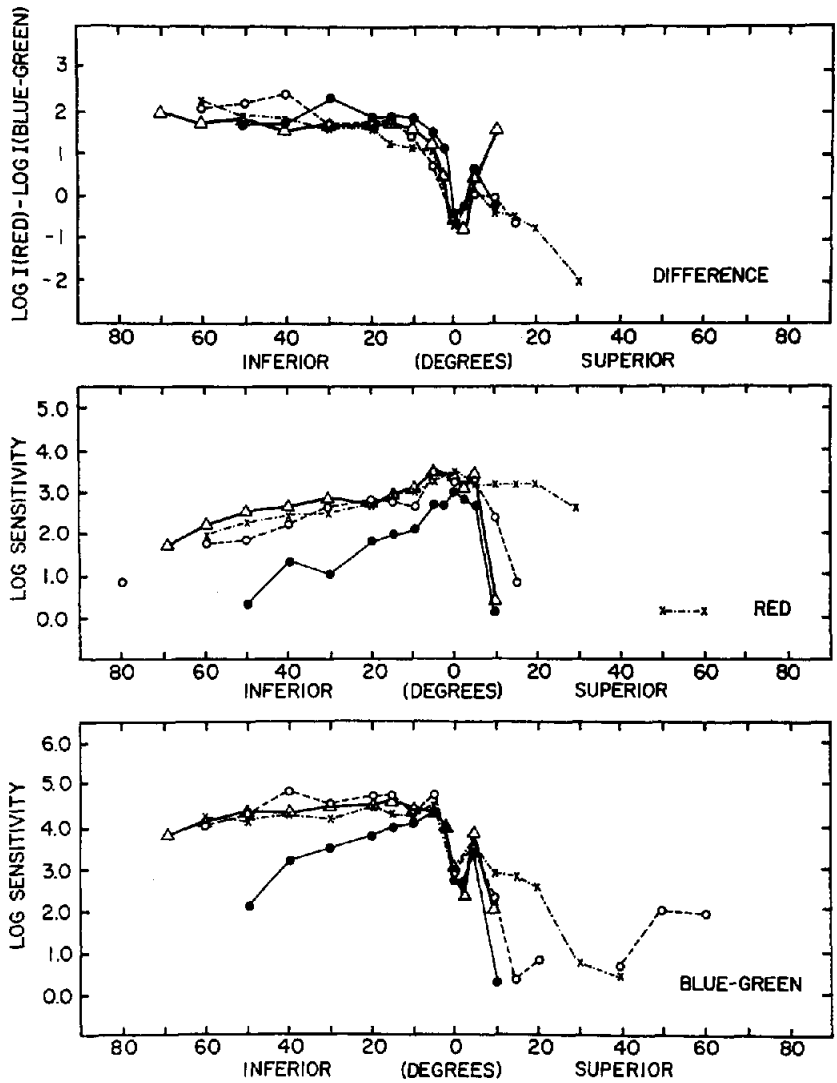

Figure 26. Log sensitivity profiles and log threshold luminance difference along the vertical meridian are plotted for four sector RP patients, from the same dominant pedigree (from Massof & Finkelstein, 1979b).

field, and the corresponding log threshold luminance difference values are at the rod level.

Patient M3 (open circles) has severe sensitivity depressions (3.5 to 5 log units) for the central 10°, and log threshold luminance difference values at the cone level. No thresholds could be measured outside the central field

except for the far inferior field (Fig. 25a); the log threshold luminance difference value for that point is at the rod level.

The three patients in this pedigree (M) illustrate field loss progression consistent with measured disease duration, but paradoxical sensitivity losses. The oldest patient (M2) has normal sensitivities, despite the field contraction. Even with the ambiguous log threshold luminance difference profiles, these patients as a group display the hallmark features of type 2; that is, there appear to be regionalized sensitivity losses, and the difference profiles indicate combined losses of rod and cone sensitivity, although some cones appear to persist in the case of severe sensitivity losses.

Comments. On the basis of threshold profiles, the type 2 dominant RP patients may be characterized as a regionalized and combined loss of rod and cone sensitivity. In the younger patients (see Fig. 21), the initial loss appears to occur in the mid-peripheral field, the region of the ring scotoma. With progression of the disease, the central 10° becomes more involved and the mid-peripheral sensitivity loss increases (see Fig. 24). The far periphery appears to retain some rod sensitivity, even in the oldest patients (see Fig. 25b).

When the sensitivity loss exceeds 3 log units, the log threshold luminance difference values begin to favor the cone contribution. As shown in Figure 26, this was also true for the superior field in dominant sector RP patients (Massof & Finkelstein, 1979b). It appears that rods and cones are both affected, but in advanced stages the cones 'outlast' the rods. In ultrastructural clinicopathologic studies of advanced RP retinas, distorted and swollen cone inner segments frequently are seen in areas corresponding to scotomas (Szamier et al., 1979).

In most cases, type 2 dominant RP is characterized by later onset of nightblindness than in type 1 dominant RP. From the vision threshold profiles, one might expect the nightblindness in type 2 patients to be characterized as a scotopic visual field loss, rather than as a literal scotopic blindness that may characterize the nightblindness in type 1 patients. Thus, the type 2 patients may not consider themselves nightblind until later in life when they begin to encounter functional difficulties in reduced illumination.

In contrast to type 1 patients, it appears that rod and cone function in type 2 patients is first lost in the mid-periphery at a time when the rest of the retina is relatively normal. With progression, the mid-peripheral loss worsens and the affected zone widens. As opposed to an active spreading of the loss, however, it appears that different regions are affected at different rates (cf. Fig. 24). The combined loss of rod and cone function could be due to pigment epithelial abnormalities, vascular abnormalities, or some other putative factor. Indeed, as shown in Figure 27, similar combined losses of rod and cone sensitivity are seen in patients with branch retinal vein occlusion (Starr, 1980).

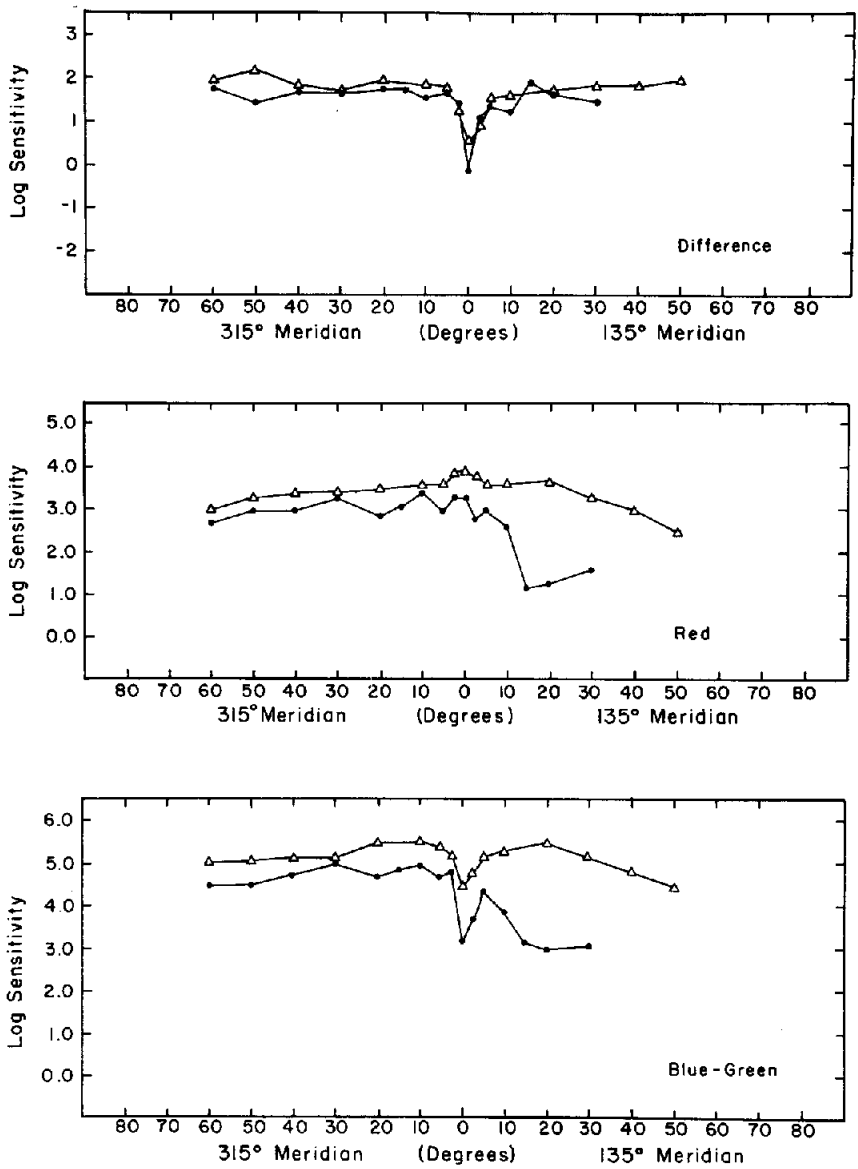

Figure 27. Log sensitivity and log threshold luminance difference profiles along the 315°/135° meridian are plotted for a patient with branch retinal vein occlusion. The area of capillary nonperfusion begins at about 5° and extends away from fixation along the 135° half-meridian. As seen in the top panel, even in regions where sensitivity losses are as great as 2.5 log units, the log threshold luminance difference value is at the rod spectral sensitivity level of 2 (e.g., 20° along the 135° half-meridian). This result indicates that there must have been a concomitant loss of rod and cone sensitivity in the region of capillary nonperfusion (from Starr, 1980).

The electroretinogram

The two dominant RP types have been identified and characterized on the basis of perimetric psychophysical studies. The electroretinogram (ERG) has been a popular clinical measure in the study of RP. Unfortunately, early in the course of the disease the ERG amplitude may become too small to record, limiting its value as a diagnostic research tool. Given the knowledge we have gained about the dominant RP subtypes, however, the ERG can serve as a corroborative measure in the few patients who have recordable retinal potentials.

Methods

The electroretinogram was recorded from the 25 patients using a Burian-Allen electrode and a ganzfeld stimulus presentation. The 'scotopic' ERG was recorded in response to a 0.5 $\mu J/cm^2$-sr, 10 μsec xenon flash on a dark background (i.e., setting 16 on a Grass PS-22 photostimulator illuminating the interior of a diffusing sphere) after 30 minutes of dark adaptation. The 'photopic' ERG was recorded similarly, but in response to the xenon flash on a 2 cd/m^2 white ganzfeld background. The scotopic ERG amplitudes (measured from the trough of the a-wave to the peak of the b-wave) are entered in Table 2; if the ERG was not recordable, NR is entered.

Results

Of the 25 RP patients described in this study, the ERG was not recordable (signal buried in the baseline noise) in 15 patients (60%). Both scotopic and photopic ERGs could be measured in 8 patients (32%); the scotopic ERG only could be measured in the remaining 2 patients (8%).

In normal subjects the scotopic ERG represents predominantly a rod system response and the photopic ERG represents predominantly a cone system response. If type 1 dominant RP patients suffer a rod system loss, while maintaining relatively intact cone function, then we would expect the scotopic ERG to be affected more than the photopic ERG. In contrast, for type 2 dominant RP patients, who appear to have a combined loss of rod and cone function, we would expect to see the scotopic and photopic ERGs to be reduced by about the same factor. Figure 28 illustrates the ratio of the photopic ERG amplitude to the scotopic ERG amplitude (each expressed as a percent of the normal mean) as a function of scotopic b-wave amplitude (the normal mean scotopic b-wave amplitude is 500 μV with $\sigma = 100\,\mu$V) for the eight patients from whom both types of ERG could be recorded.

Ratios less than 1.0 indicate a greater photopic than scotopic ERG loss, whereas ratios greater than 1.0 indicate greater scotopic than photopic ERG loss. A ratio of 1.0 would indicate an equal percent loss in both photopic and scotopic ERGs.

The type 1 dominant RP patients (open circles) have ratios ranging from 2

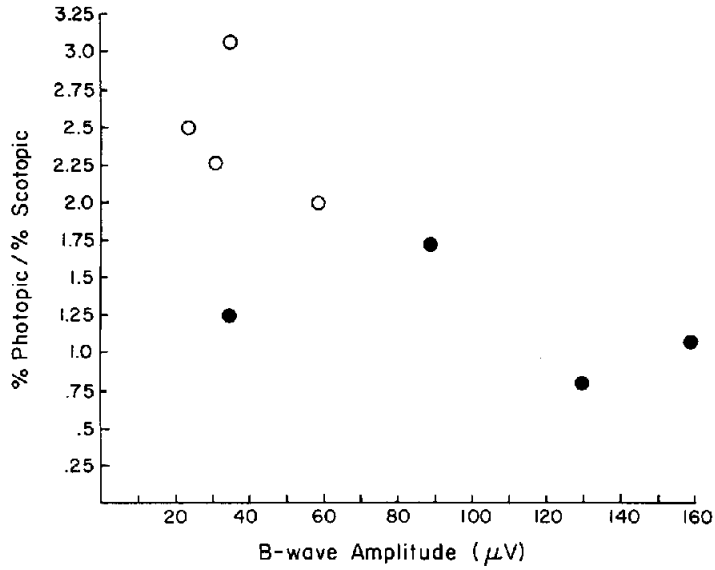

Figure 28. The ratio of photopic ERG amplitude to scotopic ERG amplitude (computed as percent of respective normal amplitudes) is plotted as a function of scotopic b-wave amplitude for type 1 (open circles) and type 2 (filled circles) dominant RP patients. A greater reduction in the photopic ERG than scotopic ERG would produce a ratio less than 1.0; a greater reduction in the scotopic ERG than in the photopic ERG would produce a ratio greater than 1.0; an equal reduction in photopic and scotopic ERGs would produce a ratio of 1.0.

to 3. These ratios indicate a greater scotopic ERG loss than photopic ERG loss and are in agreement with the previously described psychophysical measures. The type 2 dominant RP patients (closed circles) have ratios ranging from 0.8 to 1.7. Three of the four type 2 patients have ratios very close to 1, indicating an equal loss of rod and cone ERG amplitude. The fourth type 2 patient has a ratio of 1.7, indicating a somewhat greater rod loss than cone loss, but still below the values for type 1 patients. The ERG results for the type 2 RP patients also corroborate data from the psychophysical studies. (To epitomize the dichotomy between these groups, note the data for the two patients who have 35 μV scotopic ERG amplitudes; the type 1 patient has a ratio of 3.05 and the type 2 patient has a ratio of 1.25.)

Photopic b-wave implicit time (i.e. b-wave peak latency) is plotted as a function of scotopic b-wave implicit time for each patient in Figure 29. No consistent difference is seen between the two types of dominant RP patients. Two type 2 patients (closed circles) and one type 1 patient (open circles) have delayed photopic implicit times, and one type 1 patient and one type 2 patient have delayed scotopic implicit times. However, two type 2 patients have faster than normal photopic implicit times, three type 1 patients have

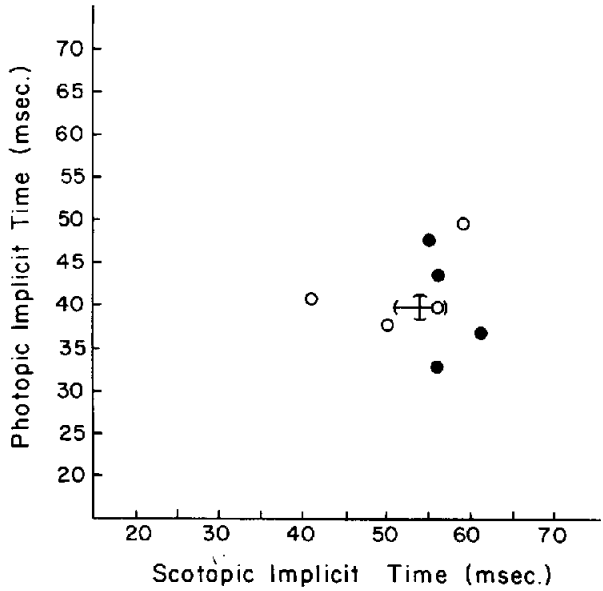

Figure 29. Implicit time of the photopic ERG b-wave is plotted as a function of the implicit time of the scotopic ERG b-wave for type 1 (open circles) and type 2 (filled circles) dominant RP patients. The elliptical cross defines the normal mean ± one standard deviation.

normal photopic implicit times, and one type 1 patient has a faster than normal scotopic implicit time.

Comment

The ERG amplitude data are in complete agreement with the conclusions drawn from the psychophysical studies, viz. type 1 patients are characterized by a rod function loss with preserved, albeit not necessarily normal cone function and type 2 patients are characterized by a combined loss of rod and cone functions. There is no consistent pattern seen in the implicit time data.

Clinical characteristics of the dominant RP subtypes

Careful fundus examinations were performed after identification of the stimulus threshold pattern and after biasing of the examiner with the knowledge of the subclassification assigned to the patient. On the basis of fundus appearance, we could not identify any unique features that could aide in differentiating the two groups of dominant RP patients. The two groups, however, exhibit a striking difference in the reported age of nightblindness

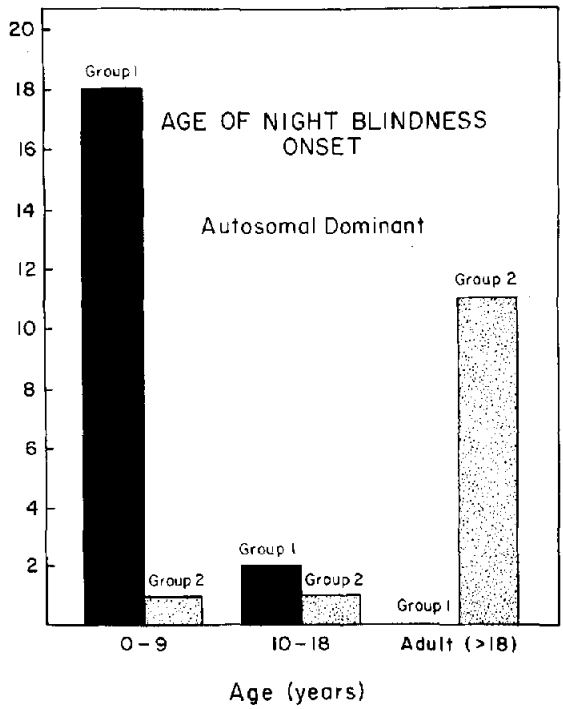

Figure 30. Histograms representing age of nightblindness onset for type 1 (solid bars) and type 2 (stippled bars) dominant RP patients.

onset. Figure 30 illustrates histograms of age of nightblindness onset, as reported by the patient. Nightblindness appears to begin in childhood for dominant type 1 and in adulthood for dominant type 2.

Visual field areas for the Goldmann V/4 target were measured with a planimeter and are plotted as a function of patient age for groups 1 and 2 in Figures 31 and 32, respectively. There is a sharp drop in visual field area for type 1 patients (Fig. 31) that occurs between age 30 and 40. Although the field loss on superficial consideration seems to be catastrophic, it may instead represent a progressive, but fairly diffuse, loss of peripheral cone sensitivity (cf. Fig. 11). Then, at some later time, cone contrast threshold may fall below the level of the V/4 target, thus contracting fields from a relatively normal size to the central 10° that remains largely unaffected.

For type 2 dominant RP (Fig. 32), the fields remain fairly large until late in the course of the disease. The early field loss that does occur (60° to 70° radius) results largely from the ring scotoma. Two patients over 55 years of age had close to 70° fields, and 3 patients over 55 years had contracted fields.

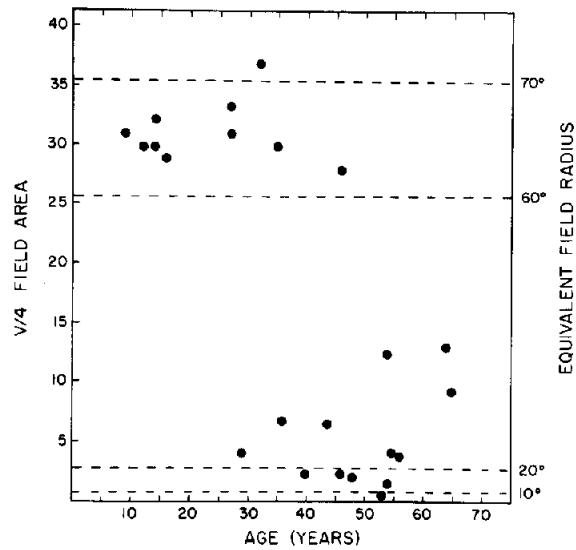

Figure 31. Area of the visual field for the V/4 target, determined by planimetry, is plotted for type 1 dominant RP patients (filled circles), as a function of patient age. For reference, broken lines represent areas of circular visual field with the radii specified on the right-hand ordinate. The normal visual field has an area greater than 40 units.

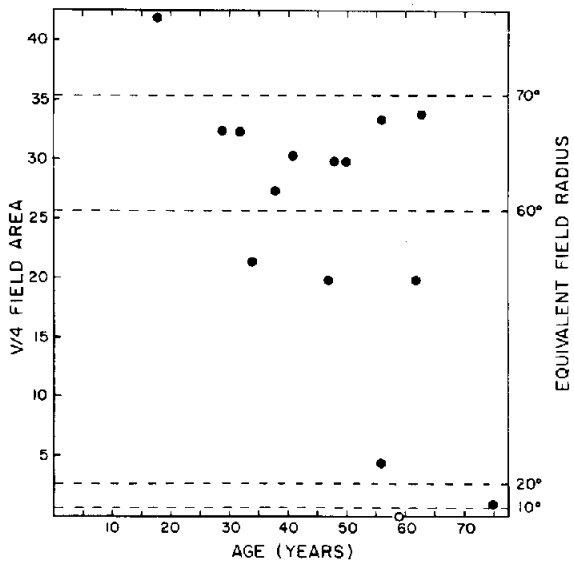

Figure 32. Same as Figure 31, but for type 2 dominant RP patients. The patient represented by the open circle had light perception only, with no definable field projection.

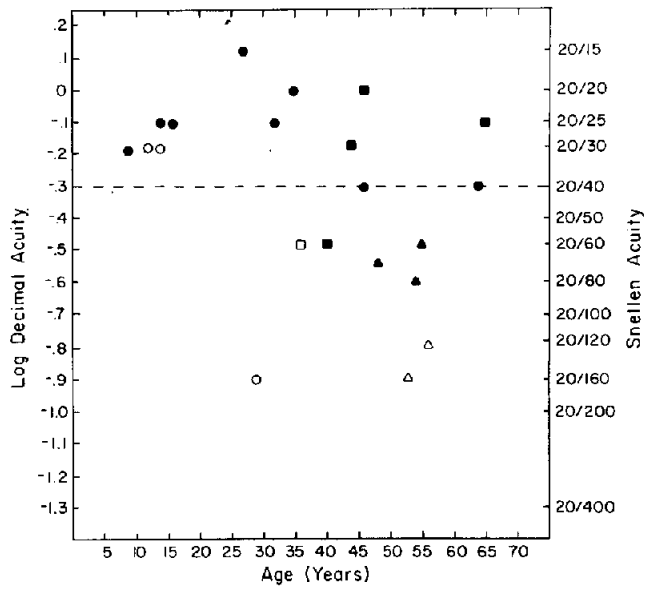

Figure 33. Corrected log decimal acuity is plotted as a function of patient age for type 1 dominant RP patients. Filled symbols denote normal-appearing macula, and open symbols denote cystoid macular edema. Circles denote clear lens; squares denote 1+ posterior subcapsular cataract (PSC); triangles denote 2+ PSC. Acuities in Snellen notation are indicated on the right-hand ordinate.

The 59-year-old patient denoted by the open circle had light perception only (this patient is a member of pedigree J). Thus, even though it would appear that group 2 patients have a better chance than group 1 patients of preserving peripheral vision until late in life, the prognosis cannot be certain.

For both groups of patients, it appears that central cone thresholds remain good throughout the course of the disease. Figures 33 and 34 illustrate visual acuity as a function of age of the patient for type 1 and 2, respectively. The filled symbols indicate that the macula appeared normal, and the open symbols denote cystoid macular edema. The circles represent a clear lens; the squares and triangles denote 1+ and 2+ posterior subcapsular cateracts, respectively. For type 1 dominant RP (Fig. 33), all patients with visual acuity worse than 20/40 have lens opacities, or visible cystoid macular edema, or both. Otherwise, there are examples of type 1 RP patients as old as 65 years who still exhibit normal visual acuity.

For type 2 (Fig. 34), the distribution of visual acuities is similar to type 1. However, unlike the type 1 group, several patients with clear media and normal macular appearance fall below 20/40 acuity. This is consistent with macular encroachment of the primary degenerative process (e.g., see Fig. 24).

Comment. Because of the relatively small number of patients in this sample, the natural history descriptions must be considered preliminary.

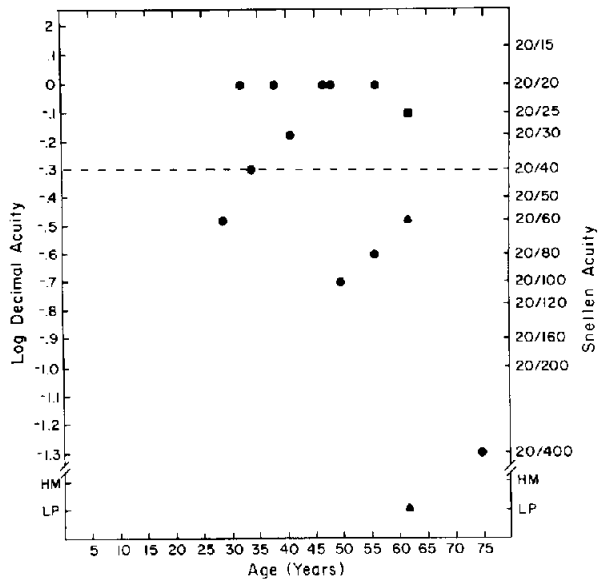

Figure 34. Same as Figure 33, but for type 2 dominant RP patients. (Symbols have the same meaning as in Figure 33; HM denotes hand-motion vision and LP denotes light perception.)

Nevertheless, the difference in age of nightblindness onset, although not revealing a perfect dichotomy between the two types, is of compelling interest and it merits attention.

General discussion

On the basis of psychophysical measures of rod and cone sensitivity loss, we have demonstrated that there are at least two types of autosomal dominant primary retinitis pigmentosa. The first type of dominant RP is characterized by an early and diffuse loss of rod sensitivity with a later progression of cone sensitivity loss. These type 1 patients usually report congenital or childhood onset of nightblindness. Type 2 dominant RP is characterized by a regionalized and combined loss of rod and cone sensitivity. In the type 2 category, for younger patients, the most severe sensitivity losses are confined to a mid-peripheral ring from 15° to 40°. With progression, the mid-peripheral sensitivity loss worsens and the central 20° becomes affected. Type 2 patients usually report adulthood onset of nightblindness.

In previous reports we have described these type 1 and type 2 threshold patterns and the corresponding dichotomy in nightblindness onset for simplex and recessive cases, and also the dominant subtypes reported here (Massof & Finkelstein, 1979a; Massof & Finkelstein, 1981). Corroboration for these findings can be found in an earlier study of RP patients by Zeavin

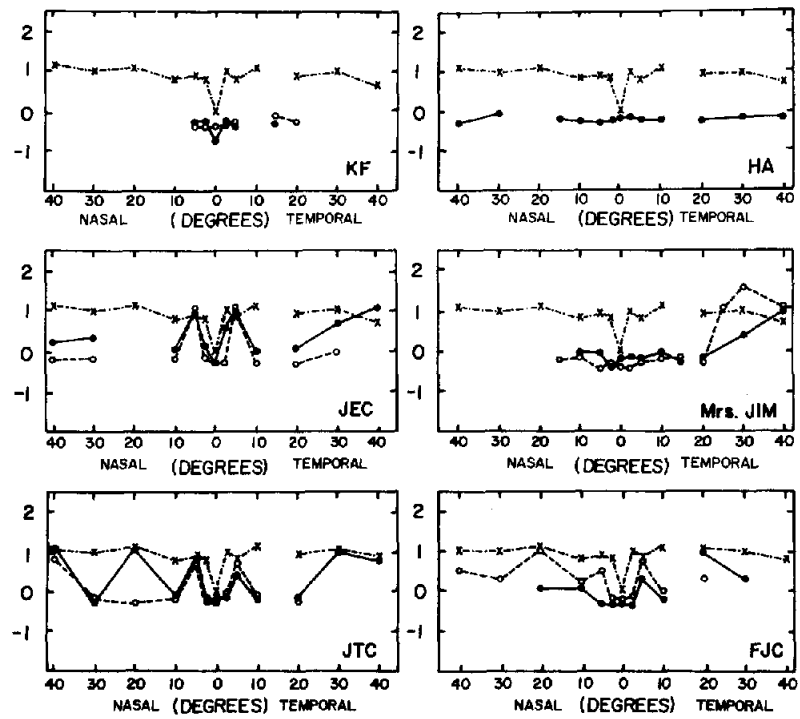

Figure 35. Log threshold luminance difference profiles are plotted for 6 patients reported by Zeavin & Wald (1956). In each panel the x's denote the normal log threshold luminance difference values, computed from the normal threshold data presented by Zeavin & Wald. Note that a log threshold luminance difference value of 0 denotes cone spectral sensitivity, and a log threshold luminance difference value of 1.0 denotes rod spectral sensitivity. The rod difference for Zeavin & Wald was 1 log unit less than the rod difference value of this study, because the stimuli they employed were closer together spectrally.

and Wald (1956); they measured absolute threshold profiles in the central 40° (radius) with an orange stimulus and a blue stimulus. Figure 35 illustrates log threshold luminance difference profiles that we computed from the published data for their six patients; mean values for their normal observers also are plotted for comparison. Their patients JEC, JTC and FJC, siblings from a presumed dominant pedigree, display a type 2 difference profile. Although no nightblindness onset data were reported for JTC or FJC, JEC was asymptotic at age 18. Patient HA, age 51, has a type 1 difference profile. Consistent with type 1 RP patients, patient HA had been nightblind since birth. Zeavin and Wald considered patient HA 'atypical' because of what appeared to be 'an apparently complete loss of rod vision associated with apparently normal cone vision'. No family history was provided for patient HA or for patients KE and JIM.

Further corroboration of the subclasses described in this paper can be

found in an ERG study of Armington et al. (1961); they reported that with ERG measures of spectral sensitivity, three RP patients had a photopic-like spectral sensitivity function (maximum sensitivity at 550 nm) and three patients had a scotopic-like spectral sensitivity function (maximum sensitivity at 490 nm). These data agree with our ERG data from type 1 and type 2 dominant RP patients, where the photopic and scotopic ERGs were affected differently in the two groups.

The pedigrees described in the present paper would be classified as having dominant RP with full penetrance. We emphasize that the two groups described in this paper represent subclassifications of the full penetrance genetic category only.

We believe that there may be at least two separate types of dominant primary retinitis pigmentosa. Type 1 and type 2 dominant RP are differentiated on the basis of: rod sensitivity loss relative to cone sensitivity loss, diffuse versus regionalized early sensitivity losses, and childhood versus adulthood nightblindness onset. We propose that type 1 and type 2 dominant RP may represent retinal degenerative diseases of separate underlying mechanism. This subclassification may become important to future research studies involving etiologic factors in retinitis pigmentosa.

Acknowledgements

The authors are grateful for the assistance provided by Rosalind Palmer, Carolyn Perry, Mary A. Johnson, Stuart J. Starr, F.W. Fitzke, Kathleen Wilson and J. David Andrews.

References

Armington JC, Gouras P, Tepas DI and Gunkel R (1961) Detection of the electroretinogram in retinitis pigmentosa. Exp Eye Res 1: 74–80

Berson EL, Gouras P and Gunkel RD (1968) Rod responses in retinitis pigmentosa, dominantly inherited. Arch Ophthal 80: 58–67

Berson EL, Gouras P, Gunkel RD and Myrianthopoulos NC (1969) Dominant retinitis pigmentosa with reduced penetrance. Arch Ophthal 81: 226–234

Fitzke FW and Massof RW (1980) Absolute cone thresholds derived from the Ferry-Porter law. Invest Ophthal Vis Sci Suppl: 212

Guth SL and Lodge HR (1973) Heterochromatic additivity, foveal spectral sensitivity, and a new color model. J Opt Soc Amer 63: 450–462

Hussels-Maumenee I, Pierce ER, Bias WB and Schleutermann DA (1975) Linkage studies of typical retinitis pigmentosa and common markers. Amer J Hum Genet 27: 505–508

Jay B (1972) Hereditary aspects of pigmentary retinopathy. Trans Ophthal Soc UK 92: 173–178

Johnson MA & Massof RW (1980) The photochromatic interval in the peripheral retina. Recent Advances in Vision Tech Digest. Optical Society of America, Washington.

Krill AE (1972) Retinitis pigmentosa: a review. Sightsav Rev 42: 21–28

Marmor MF (1979) The electroretinogram in retinitis pigmentosa. Arch Ophthal 97: 1300–1304

Massof RW and Finkelstein D (1979a) Rod sensitivity relative to cone sensitivity in

retinitis pigmentosa. Invest Ophth Vis Sci 18: 263–272
Massof RW and Finkelstein D (1979b) Vision threshold profiles in sector retinitis pigmentosa. Arch Ophthal 97: 1899–1904
Massof RW and Finkelstein D (1981) Subclassifications of retinitis pigmentosa from two-color scotopic static perimetry. Docum Ophthal Proc Ser 26: 219–225
Massof RW, Johnson MA and Finkelstein D (1981) Peripheral absolute threshold spectral sensitivity in retinitis pigmentosa. Brit J Ophthal 65: 112–121
Palmer RW, Massof RW and Finkelstein D (1980) Heterogeneity within subgroups of retinitis pigmentosa. Invest Ophthal Vis Sci Suppl: 90
Stabell U and Stabell B (1981) Spectral sensitivity of the dark-adapted extrafoveal retina at photopic intensities. J Opt Soc Amer 71: 841–844
Starr SJ (1980) Rod sensitivity relative to cone sensitivity in retinal vascular disease. Invest Ophthal Vis Sci Suppl: 78
Szamier RB, Berson EL, Klein R and Meyers S (1979) Sex-linked retinitis pigmentosa: ultrastructure of photoreceptors in pigment epithelium. Invest Ophthal Vis Sci 18: 145–160
Wooten BR, Fuld K and Spillmann L (1975) Photopic spectral sensitivity of the peripheral retina. J Opt Soc Amer 65: 334–342
Zeavin BH & Wald G (1956) Rod and cone vision in retinitis pigmentosa. Amer J Ophthal 42: 253–269